
A HYBRID ABM-PDE FRAMEWORK FOR REAL-WORLD INFECTIOUS DISEASE SIMULATIONS

A PREPRINT

Kristina Maier
Zuse Institute Berlin
Berlin, 14195
maier@zib.de

Tim O. F. Conrad
Zuse Institute Berlin
Berlin, 14195
conrad@zib.de

ABSTRACT

This paper presents a hybrid modeling approach that couples an Agent-Based Model (ABM) with a partial differential equation (PDE) model in an epidemic setting to simulate the spatial spread of infectious diseases using a compartmental structure with seven health states. The goal is to reduce the computational complexity of a full-ABM by introducing a coupled ABM-PDE model that offers significantly faster simulations while maintaining comparable accuracy. Our results demonstrate that the hybrid model not only reduces the overall simulation runtime (defined as the number of runs required for stable results multiplied by the duration of a single run) but also achieves smaller errors across both 25% and 100% population samples.

The coupling mechanism ensures consistency at the model interface: agents crossing from the ABM into the PDE domain are removed and represented as density contributions at the corresponding grid node, while surplus density in the PDE domain is used to generate agents with plausible trajectories derived from mobile phone data.

We evaluate the hybrid model using real-world mobility and infection data for the Berlin–Brandenburg region in Germany, showing that it captures the core epidemiological dynamics while enabling efficient large-scale simulations.

Keywords Partial differential equation · epidemic modeling · spatial modeling · coupling approach · diffusion · agent-based model · landscape

1 Introduction

Understanding and efficiently simulating complex dynamical systems is a central challenge across many scientific and engineering domains. In epidemiology, this challenge is particularly pronounced due to the need to capture diverse phenomena such as individual behavior, spatial mobility, and population heterogeneity. In this field, various modeling approaches exist, such as agent-based models (ABMs) [23], models based on partial differential equations (PDEs) [11], and ordinary differential equation (ODE) models [32]. Each of these approaches offers distinct advantages: ABMs provide detailed individual-level dynamics but are computationally demanding; ODEs are efficient and analytically tractable but lack spatial structure; PDEs incorporate spatial variation, which is critical for modeling heterogeneous regions.

Each of these modeling approaches has its place, but choosing the most appropriate one often depends on the characteristics of the domain being studied. In practice, however, many real-world regions exhibit a mix of features that make a single modeling paradigm insufficient. Consider, for instance, the Berlin–Brandenburg region: while Berlin represents a densely populated, relatively homogeneous urban area, Brandenburg is more rural and spatially heterogeneous. Applying the same model across both regions may either introduce unnecessary complexity or overlook important spatial effects. To address this, we adopt a hybrid modeling approach that assigns different models to distinct, non-overlapping subregions – each selected to best capture the local dynamics. This strategy allows us to leverage the respective strengths of each modeling framework while maintaining consistency across the overall system.

Hybrid modeling approaches combining ABMs and PDEs have been employed in other scientific domains, such as cellular biology and oncology; however applications in the context of human-to-human disease transmission remain rare. For instance, Kostre et al. [17] apply hybrid ABM-PDE models to simulate biochemical processes at the cellular level, modeling interactions between molecules and cells through coupled particle-based simulations and reaction-diffusion PDEs. Particles diffuse within the particle domain. Upon crossing the boundary into the concentration domain, they are eliminated. The concentration at the boundary of the PDE domain is converted into virtual particles and fractional virtual particles, which can jump into the particle domain at a certain rate. Similar ABM-PDE hybrids have been used to investigate viral dynamics in cell populations [21], antiviral drug effects [15], and treatment strategies in oncology [28].

Recent studies have also explored machine learning techniques to construct surrogate models that approximate behaviour of detailed ABMs [4]. These data-driven approaches – often based on neural networks – can replicate complex ABM dynamics with significantly reduced computational cost, enabling more efficient parameter calibration and sensitivity analyses. As such, they offer a promising approach for enabling large-scale simulations. However, a key limitation of these methods lies in their lack of interpretability – an important drawback in epidemiological applications, where understanding the underlying mechanisms is essential for informed public health decision-making.

In this study, we present and evaluate a hybrid ABM-PDE model using real-world data, specifically applied to the Berlin-Brandenburg region. The model incorporates real-world mobile phone data, representing 25% and 100% of the population, capturing realistic movement patterns crucial for disease dynamics modeling. The model’s evaluation is based on real-world infection data and compared to a high-resolution, full-ABM simulation that serves as a reference. Our hybrid approach enables the exchange of information between the two (sub-)models at each time step, ensuring a dynamic yet consistent interaction between local and global disease dynamics.

The resulting hybrid ABM-PDE model provides a faster alternative to a full-ABM model, offering the benefit of quicker parameter fitting due to reduced overall simulation runtime, regardless of whether the 25% or 100% population sample is used. Furthermore, the hybrid model demonstrated better accuracy over short simulation horizons – approximately two months –, when fitting was done for two separate intervals. The underlying ABM is a streamlined version of EpiSim [1] implemented in C++, and is capable of simulating 100% of the population on a standard computer.

Building on these results, our long-term objective is to extend the current hybrid framework into a comprehensive ABM-PDE-ODE coupled model, which will integrate previous advancements in ABM-ODE [8] and PDE-ODE coupling [20].

The complete model implementation and the processed infection data from the Robert Koch Institute (RKI) website are available on Zenodo¹. Mobility data is available from the authors upon reasonable request.

2 Model Formulation

Our proposed hybrid model couples an agent-based model (ABM) and a partial differential equation (PDE) model to simulate the spatial spread of infectious diseases in the Berlin-Brandenburg region. The urban area of Berlin is represented by a PDE model that captures population-level dynamics and health state transitions, while the surrounding rural area of Brandenburg is modeled using an ABM based on real-world individual movement data from mobile phones. The data used for the ABM consists of individuals who have been in Berlin or Brandenburg at least once, with a few individuals from outside the region. For simplicity, we refer to the entire modeling domain as Brandenburg for the hybrid model.

Both models incorporate different epidemiological health states, and are dynamically coupled at each time step: individuals crossing the boundary are either removed from the ABM and added to the PDE as density contributions, or generated in the ABM from excess density in the PDE. This exchange ensures consistency across the boundary and reflects observed mobility patterns.

The remainder of this section is structured as follows:

- Part 1 introduces the PDE-based compartment model for Berlin (Section 2.1).
- Part 2 presents the trajectory-driven ABM for Brandenburg, based on mobile phone data (Section 2.2).
- The initialization – or setting of initial conditions – of both model component is described in Section 2.3.
- Finally, Section 2.4 explains the coupling mechanism that integrates both parts into a single hybrid simulation framework.

¹<https://zenodo.org/records/15100902>

2.1 Part 1: Berlin – PDE-Based Compartment Model

To model disease dynamics in the urban region of Berlin, we derive a PDE system from a motion-based ABM that incorporates individual movement guided by a spatial landscape and includes health state transitions. This approach allows us to capture spatially continuous population dynamics while maintaining a structured epidemiological model. Several methods exist for deriving a (stochastic) PDE system from an ABM (with multiple states) (e.g. [14, 24]). In our work, we follow the approach proposed by Helfmann et al. [14], in which the authors show how to translate agent motion and state transitions into a system of stochastic PDEs. We proceed as follows: we first define a motion-based ABM with a single state using a landscape to guide spatial movement. We then extend the model to include multiple health states and associated transitions between them. Next, we translate (reduce) this into a PDE-based compartment model, and finally, we present its weak formulation to enable numerical simulation using the finite element method.

2.1.1 Construction of the Motion-Based ABM

The overall aim is to construct an ABM consisting of agents moving stochastically and continuously within a domain, described by Brownian motion and a landscape in which agents can change their health status probabilistically, influenced by the health status of their neighbors. The first step is to construct a motion-based ABM in which agents move stochastically and continuously within a spatial domain. Each agent’s movement is governed by Brownian motion influenced by a landscape potential, which guides them toward frequently visited areas. So for now, we focus only on mobility — no health state transitions are considered yet. The domain $\Omega_{Be} \subseteq \mathbb{R}^2$ represents the urban area of Berlin. The landscape V defines spatial preferences and is specified on an equidistant grid. Because agents move in continuous space, the local value of V at their current grid cell influences the agent’s next movement.

To model the agent’s movement, we consider an overdamped Langevin diffusion process [19] following the approach of Helfmann et al. [14], which describes the evolution of an agent’s position $X(t) \in \mathbb{R}^2$ over time t as:

$$dX(t) = -\nabla V(X(t))dt + \sqrt{2D} dB(t),$$

where $V : \Omega_{Be} \rightarrow \mathbb{R}$ is the landscape potential, $D \in \mathbb{R}$ is the diffusion coefficient, and $B(t) \in \mathbb{R}^2$ denotes a standard Brownian motion. The drift term $-\nabla V(X(t))$ causes agents to preferentially move toward regions of lower potential, which correspond to areas with higher empirical presence in the underlying data.

We exploit the property of the system that the landscape $V : \Omega_{Be} \rightarrow \mathbb{R}$ can be expressed as

$$V(X) = -\left(\frac{D}{2}\right) \log(p_{st}(X)), \quad (1)$$

where $p_{st}(X)$ is the probability distribution of the agents at location X [19]. To approximate the probability distribution of the agents at each location, we use mobile phone data. First, we generate agent trajectories by determining their location for each hour of the day. Next, we aggregate all trajectories for each hour of the day over the entire week to construct a histogram. After normalization, this histogram represents the probability distribution of the agents, which we use to compute the landscape. Mobile phone data is available for Berlin and Brandenburg, so the landscape is initially defined for the entire region, and then we extract the portion corresponding to Berlin.

Our motion-based ABM for agent $i = 1, 2, \dots, N_a$ is then given by the overdamped Langevin diffusion equation system

$$dX_i(t) = -\nabla V(X_i(t))dt + \sqrt{2D} dB_i(t).$$

2.1.2 Extension with Health States

We now extend the motion-based ABM by introducing multiple health states and transition rules to capture the dynamics of infectious disease progression. The population is divided into subpopulations, each associated with a distinct epidemiological status. These statuses and their transitions are modeled via a set of interaction rules $\mathcal{R} = (\mathcal{R}_r)_{r=1}^{10}$, following Helfmann et al. [14] and the work by Müller and colleagues [22, 23] for the epidemiological assumptions:

$$\begin{array}{ll} \mathcal{R}_1 : & T_S + T_{E \cup I} \rightarrow 2T_E \\ \mathcal{R}_2 : & T_E \rightarrow T_I \\ \mathcal{R}_3 : & T_I \rightarrow T_R \\ \mathcal{R}_4 : & T_I \rightarrow T_{S_Y} \\ \mathcal{R}_5 : & T_{S_Y} \rightarrow T_R \\ \mathcal{R}_6 : & T_{S_Y} \rightarrow T_H \\ \mathcal{R}_7 : & T_H \rightarrow T_R \\ \mathcal{R}_8 : & T_H \rightarrow T_C \\ \mathcal{R}_9 : & T_C \rightarrow T_{H_C} \\ \mathcal{R}_{10} : & T_{H_C} \rightarrow T_R, \end{array} \quad (2)$$

where T_Y describe the different agent types with $Y \in \{S, E, I, {}^S Y, H, C, H_C, R\}$. The health statuses are defined as follows:

- susceptible (S)
- exposed (E) - not symptomatic, not infectious
- infectious (I) - not symptomatic, infectious
- symptomatic (${}^S Y$) - symptomatic, infectious
- requiring hospitalization (after being symptomatic before) (H)
- critical (C)
- requiring hospitalization (after being in critical state before) (H_C)
- recovered (R).

The agent type or state of agent i at time t is defined as $Y_i(t)$. The total number of people requiring hospitalization is the sum of agents that are in state H or H_C . The total number of infected people is the sum of agents that are in state $E, I, {}^S Y, H, C$ or H_C . We define the total number of all agents as N . We do not consider deaths or births, i.e., our total population N remains constant with respect to time.

State transitions (health status change) occur at discrete time points $t_k, k = 1, 2, \dots, K$, with constant time step size Δt . The probability of a health status change for agent i at time t_k is given by:

$$1 - \exp\left(-\Delta t \sum_{r \in \mathcal{R}} \lambda_i^r(t_k)\right), \quad k = 1, \dots, K,$$

where the transition rate function $\lambda_i^r(t)$ of agent $i = 1, \dots, N_a$ and rule $r = 1, \dots, 10$ at time t is given by

$$\lambda_i^r(t) = \mathcal{T}_r \mathbb{1}_{Y'}(Y_i(t)) \sum_{j=1}^N A_{ij}(t) \mathbb{1}_{Y''}(Y_j(t)), \quad Y', Y'' \in \{S, E, I, {}^S Y, H, C, H_C, R\}$$

[14]. Further, we have the constant transition rates \mathcal{T}_r for each rule r , characteristic function $\mathbb{1}_{\{\cdot\}}$, and an adjacency matrix

$$A(t) = (A_{ij}(t))_{i,j=1}^{N_a} = \begin{cases} 1 & \text{if } \|X_i(t) - X_j(t)\| \leq d_{int} \text{ for } i \neq j \\ 0 & \text{else} \end{cases}$$

where d_{int} is a predefined distance threshold, such that agents are considered close enough to transmit the disease. If multiple transitions are possible for an agent, the specific rule is chosen with probability

$$\frac{\lambda_i^r(t_k)}{\sum_{r \in \mathcal{R}} \lambda_i^r(t_k)}.$$

In some cases, such as for *susceptible* (S) or *critical* (C) agents, only one rule applies, so the next state is uniquely determined (to *exposed* (E) or *requiring hospitalization* (H_C), respectively).

2.1.3 Derivation of the PDE System

Each compartment in the PDE model represents the spatial density of individuals in a given health state, evolving over time. Health state transitions are incorporated through reaction terms in the PDEs, analogous to compartmental models. For example, the transition from exposed E to infectious I is governed by a loss term $\sigma E(x, t)$ in the equation for E , and a corresponding gain term in the equation for I . Similarly, new infections appear as a loss in the susceptible density and a gain in the exposed compartment, driven by contact with nearby infectious individuals. This structure allows the PDE model to capture both spatial movement and disease progression through the population. A schematic overview of the compartment structure and health state transitions is shown in Figure 1.

Building on the rules (2) from Section 2.1.2 and following the approach by Helfmann et al. [14], we now derive the system of stochastic PDEs governing the spatially distributed health compartments. The resulting stochastic PDE system reflects the combined effects of agent motion (via diffusion and drift in the landscape), state transitions (as reaction terms), and intrinsic stochasticity (representing random fluctuations in agent movement and interactions, modeled through multiplicative white noise terms in the PDE system).

Note that each compartment $X(x, t) \in S, E, I, S^Y, H, C, H_C, R$ evolves according to a stochastic reaction-diffusion equation of the general form:

$$\frac{\partial X(x, t)}{\partial t} = D\Delta X(x, t) + \nabla (\nabla V(x) X(x, t)) + (\text{reaction terms}) + (\text{noise terms}).$$

Where – as before – D is the diffusion coefficient, $V(x)$ is the landscape potential, and the reaction terms are derived from the interaction rules defined in the ABM. The noise terms model stochastic fluctuations due to random movement and stochastic health status transitions at the agent level.

Following this structure, the full system of equations is given as:

$$\begin{aligned} \frac{\partial S(x, t)}{\partial t} &= D\Delta S(x, t) + \nabla (\nabla V(x) S(x, t)) + \sqrt{2D}\nabla \left(\sqrt{S(x, t)} Z^D(x, t) \right) \\ &\quad - \beta S(x, t) \left(I(t)^{B_r(x)} + S^Y(t)^{B_r(x)} \right) - \sqrt{\beta S(x, t) \left(I(t)^{B_r(x)} + S^Y(t)^{B_r(x)} \right)} Z_1^I(x, t) \\ \frac{\partial E(x, t)}{\partial t} &= D\Delta E(x, t) + \nabla (\nabla V(x) E(x, t)) + \sqrt{2D}\nabla \left(\sqrt{E(x, t)} Z^D(x, t) \right) \\ &\quad + \beta S(x, t) \left(I(t)^{B_r(x)} + S^Y(t)^{B_r(x)} \right) + \sqrt{\beta S(x, t) \left(I(t)^{B_r(x)} + S^Y(t)^{B_r(x)} \right)} Z_1^I(x, t) \\ &\quad - \sigma E(x, t) - \sqrt{\sigma E(x, t)} Z_2^I(x, t) \\ \frac{\partial I(x, t)}{\partial t} &= D\Delta I(x, t) + \nabla (\nabla V(x) I(x, t)) + \sqrt{2D}\nabla \left(\sqrt{I(x, t)} Z^D(x, t) \right) \\ &\quad + \sigma E(x, t) + \sqrt{\sigma E(x, t)} Z_2^I(x, t) - \phi_i I(x, t) - \sqrt{\phi_i I(x, t)} Z_3^I(x, t) - \gamma I(x, t) - \sqrt{\gamma I(x, t)} Z_4^I(x, t) \\ \frac{\partial S^Y(x, t)}{\partial t} &= D\Delta S^Y(x, t) + \nabla (\nabla V(x) S^Y(x, t)) + \sqrt{2D}\nabla \left(\sqrt{S^Y(x, t)} Z^D(x, t) \right) \\ &\quad + \gamma I(x, t) + \sqrt{\gamma I(x, t)} Z_4^I(x, t) - \phi_{sy} S^Y(x, t) - \sqrt{\phi_{sy} S^Y(x, t)} Z_5^I(x, t) \\ &\quad - \eta S^Y(x, t) - \sqrt{\eta S^Y(x, t)} Z_6^I(x, t) \\ \frac{\partial H(x, t)}{\partial t} &= D\Delta H(x, t) + \nabla (\nabla V(x) H(x, t)) + \sqrt{2D}\nabla \left(\sqrt{H(x, t)} Z^D(x, t) \right) \\ &\quad + \eta S^Y(x, t) + \sqrt{\eta S^Y(x, t)} Z_6^I(x, t) - \phi_h H(x, t) - \sqrt{\phi_h H(x, t)} Z_7^I(x, t) \\ &\quad - \kappa H(x, t) - \sqrt{\kappa H(x, t)} Z_8^I(x, t) \\ \frac{\partial C(x, t)}{\partial t} &= D\Delta C(x, t) + \nabla (\nabla V(x) C(x, t)) + \sqrt{2D}\nabla \left(\sqrt{C(x, t)} Z^D(x, t) \right) \\ &\quad + \kappa H(x, t) + \sqrt{\kappa H(x, t)} Z_8^I(x, t) - \eta_c C(x, t) - \sqrt{\eta_c C(x, t)} Z_9^I(x, t) \\ \frac{\partial H_C(x, t)}{\partial t} &= D\Delta H_C(x, t) + \nabla (\nabla V(x) H_C(x, t)) + \sqrt{2D}\nabla \left(\sqrt{H_C(x, t)} Z^D(x, t) \right) \\ &\quad + \eta_c C(x, t) + \sqrt{\eta_c C(x, t)} Z_9^I(x, t) - \phi_{hc} H_C(x, t) - \sqrt{\phi_{hc} H_C(x, t)} Z_{10}^I(x, t) \\ \frac{\partial R(x, t)}{\partial t} &= D\Delta R(x, t) + \nabla (\nabla V(x) R(x, t)) + \sqrt{2D}\nabla \left(\sqrt{R(x, t)} Z^D(x, t) \right) \\ &\quad + \phi_i I(x, t) + \sqrt{\phi_i I(x, t)} Z_3^I(x, t) + \phi_{sy} S^Y(x, t) + \sqrt{\phi_{sy} S^Y(x, t)} Z_5^I(x, t) \\ &\quad + \phi_h H(x, t) + \sqrt{\phi_h H(x, t)} Z_7^I(x, t) + \phi_{hc} H_C(x, t) + \sqrt{\phi_{hc} H_C(x, t)} Z_{10}^I(x, t), \end{aligned}$$

where $Z^D(x, t) \in \mathbb{R}^2$ denotes the white noise associated with diffusion and $Z_r^I(x, t) \in \mathbb{R}^2$ represents the white noise for the r^{th} interaction, where $r = 1, 2, \dots, 10$. Since the expected value of the noise is zero, the resulting system of

PDEs is given by

$$\begin{aligned}
\frac{\partial S(x,t)}{\partial t} &= D\Delta S(x,t) + \nabla(\nabla V(x)S(x,t)) - \beta S(x,t)(I(t)^{B_r(x)} + {}^S Y(t)^{B_r(x)}) \\
\frac{\partial E(x,t)}{\partial t} &= D\Delta E(x,t) + \nabla(\nabla V(x)E(x,t)) + \beta S(x,t)(I(t)^{B_r(x)} + {}^S Y(t)^{B_r(x)}) - \sigma E(x,t) \\
\frac{\partial I(x,t)}{\partial t} &= D\Delta I(x,t) + \nabla(\nabla V(x)I(x,t)) + \sigma E(x,t) - \phi_i I(x,t) - \gamma I(x,t) \\
\frac{\partial {}^S Y(x,t)}{\partial t} &= D\Delta {}^S Y(x,t) + \nabla(\nabla V(x){}^S Y(x,t)) + \gamma I(x,t) - \phi_{sy} {}^S Y(x,t) - \eta {}^S Y(x,t) \\
\frac{\partial H(x,t)}{\partial t} &= D\Delta H(x,t) + \nabla(\nabla V(x)H(x,t)) + \eta {}^S Y(x,t) - \phi_h H(x,t) - \kappa H(x,t) \\
\frac{\partial C(x,t)}{\partial t} &= D\Delta C(x,t) + \nabla(\nabla V(x)C(x,t)) + \kappa H(x,t) - \eta_c C(x,t) \\
\frac{\partial H_C(x,t)}{\partial t} &= D\Delta H_C(x,t) + \nabla(\nabla V(x)H_C(x,t)) + \eta_c C(x,t) - \phi_{hc} H_C(x,t) \\
\frac{\partial R(x,t)}{\partial t} &= D\Delta R(x,t) + \nabla(\nabla V(x)R(x,t)) + \phi_i I(x,t) + \phi_{sy} {}^S Y(x,t) + \phi_h H(x,t) + \phi_{hc} H_C(x,t).
\end{aligned} \tag{3}$$

The parameter choices are addressed in Section 3. The compartments and transition rates between compartments are

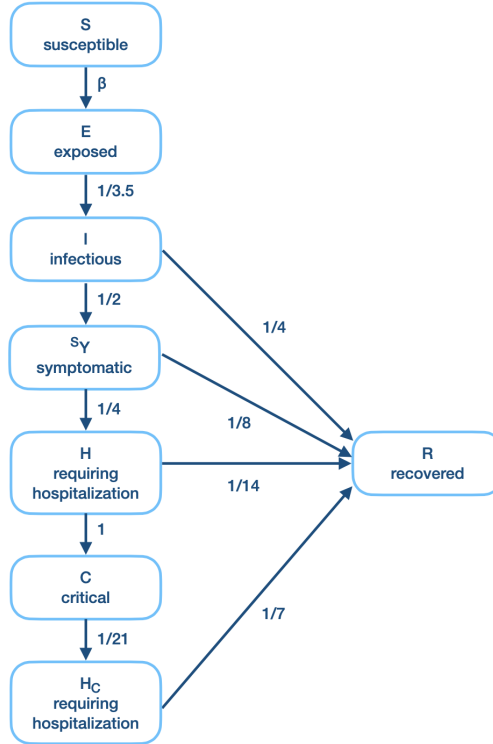


Fig. 1. Structure of the SEIYHCR model with seven health states and ten transition rules, capturing disease progression from Susceptible to Recovered via intermediate states.

displayed in Fig. 1.

Note that summing up all subpopulations results in a population movement corresponding to this PDE with a constant diffusion coefficient D

$$\frac{\partial N(x,t)}{\partial t} = D\Delta N(x,t) + \nabla(\nabla V(x)N(x,t)),$$

which is an approximation of our motion-based ABM for agents $i = 1, 2, \dots, N_a$

$$dX_i(t) = -\nabla V(X_i(t))dt + \sqrt{2D} dB_i(t).$$

2.1.4 Weak Formulation

To prepare the system of PDEs (3) for numerical simulation using the finite element method, we derive its weak formulation. This involves multiplying each equation by a test function φ and integrating over the domain Ω_{Be} . In that way, we get the weak formulation of the PDEs for the densities. For example, the PDE of susceptible density is then given by

$$\int_{\Omega_{Be}} \frac{\partial S}{\partial t} \varphi \, dx = \int_{\Omega_{Be}} -D\nabla S \cdot \nabla \varphi + \Delta V S \varphi + \frac{\partial V}{\partial x_1} \frac{\partial S}{\partial x_1} \varphi + \frac{\partial V}{\partial x_2} \frac{\partial S}{\partial x_2} \varphi - \beta S \left(\int_{B_r(x)} (I + {}^S Y) \, dy \right) \varphi \, dx.$$

Assuming the Laplacian of our landscape is zero $\Delta V = 0$, the equation reduces to

$$\int_{\Omega_{Be}} \frac{\partial S}{\partial t} \varphi \, dx = \int_{\Omega_{Be}} -D\nabla S \cdot \nabla \varphi + \frac{\partial V}{\partial x_1} \frac{\partial S}{\partial x_1} \varphi + \frac{\partial V}{\partial x_2} \frac{\partial S}{\partial x_2} \varphi - \beta S \left(\int_{B_r(x)} (I + {}^S Y) \, dy \right) \varphi \, dx.$$

Since our domain is quite large and the spatial mesh is relatively coarse, the distance between neighboring grid points is substantial – on the order of hundreds of meters. In the context of infection spreading, this implies that within a ball $B_r(x)$ of contact radius r , it is reasonable to assume that only a single grid point contributes significantly. Hence, we will approximate the integral of infectious density over the ball $B_r(x)$ by the infectious density at the center x scaled by the area of the ball

$$\int_{B_r(x)} (I(y, t) + {}^S Y(y, t)) \, dy \approx \pi r^2 (I(x, t) + {}^S Y(x, t)).$$

This localized approximation is consistent with the resolution of the spatial discretization and simplifies the infection term in the weak formulation. As such, the weak form for the susceptible compartment becomes:

$$\int_{\Omega_{Be}} \frac{\partial S}{\partial t} \varphi \, dx \approx \int_{\Omega_{Be}} -D\nabla S \cdot \nabla \varphi + \frac{\partial V}{\partial x_1} \frac{\partial S}{\partial x_1} \varphi + \frac{\partial V}{\partial x_2} \frac{\partial S}{\partial x_2} \varphi - \beta \pi r^2 S (I + {}^S Y) \varphi \, dx.$$

Analogous approximations are applied to the weak formulations of the other compartments, which follow the same structure. For implementation details, we refer to the corresponding code (see `covid.hh`).

2.2 Part 2: Brandenburg – ABM Based on Mobile Phone Trajectories

In contrast to the PDE-based model for Berlin, the Brandenburg region is represented by an *ABM* based on high-resolution mobile phone data to reconstruct realistic individual trajectories. Note that the used dataset includes individuals who have been present in Brandenburg or Berlin at least once in the recorded data, regardless of their actual place of residence.

Each agent is either located inside a facility – such as home, workplace, school or leisure facility – or commuting between facilities. While commuting, agents are assumed to be isolated and cannot transmit infections. Within facilities, agents can only interact with others inside the same facility and category. This means, infection transmission can occur only if an infectious and a susceptible agent are present in the same location of the same facility type. Health status updates happen at every time step, except for susceptible agents for which the health status is updated only upon leaving a facility. Transitions in health states follow the same rules as described in Section 2.1.2.

The mobile phone data is provided as a sequence of time-stamped events for each agent. Each event indicates either the start or end of an activity at a specific facility of a certain category. Agents are assumed to travel in straight lines between facilities, with walking speed adjusted to match the expected arrival time. We do not explicitly model other modes of transportation. Since facilities vary in size and layout, we estimate effective room sizes based on the maximum number of people present in the facility of a certain category during peak times (see Section *Estimation of room sizes* in [22, 23]). These estimates are used to approximate the density of interactions within facilities (and categories) and thus influence infection probabilities.

In addition to the baseline mobility extracted from the mobile phone dataset, the ABM incorporates mechanisms to simulate behavioral changes and policy interventions over time. One such mechanism is the use of activity change rates for out-of-home activities (see Sec. 4). These rates are defined on a daily basis and allow us to modify the original mobility data to reflect changes in social behavior, such as reduced movement during lockdowns. At the start of the simulation, the activity change rate is set to zero, meaning the input data is used as-is. On later days, if the rate becomes negative, a corresponding proportion of events (such as visits to work or leisure facilities) is randomly removed. This reduces contact opportunities while preserving the structure of the original data. If the rate becomes positive, we do not add new events, in order to avoid introducing artificial behavior not present in the original data. Policy interventions such as school closures are implemented in a similar way: if schools are marked as closed on a given day, all school-related events are excluded from the simulation for that period.

2.3 Initial Values

Agents modeled in the ABM part of the hybrid system are initialized based on their first recorded positions from the mobile phone data. In the PDE component, the initial distribution of individuals is informed by the underlying landscape, which is derived from agent movement. To use the landscape for initialization, we first shift all values so that the landscape becomes strictly positive, denoting the result as V_+ . Next, we take the inverse of V_+ , as locations with steeper landscape values correspond to areas where population density should be higher. We then normalize the inverse of V_+ to construct a probability distribution over the domain:

$$\frac{1}{V_+(x_i) \int_{\Omega_{Be}} \frac{1}{V_+(x)} dx}. \quad (4)$$

Multiplying this initial probability distribution by the total number of individuals in each health compartment yields the initial values of the PDE system as defined in equation (3).

2.4 Coupling

The coupling between the ABM and PDE components is implemented by dynamically exchanging individuals between the two model domains. When agents cross the boundary from the ABM to the PDE region, they are removed from the ABM and their health status is translated into a corresponding density contribution in the PDE. Conversely, when individuals leave the PDE region, they are instantiated as new agents in the ABM, and the corresponding amount is subtracted from the PDE densities.

To ensure well-posedness of the PDE system and avoid artificial fluxes across the boundary, we impose zero Neumann boundary conditions for the PDE contribution (3) of the hybrid model across the entire boundary:

$$D\nu^T \nabla Y = 0, \quad Y \in \{S, E, I, {}^S Y, H, C, H_C, R\}$$

where ν denotes the unit outer normal vector to the PDE domain Ω_{Be} . Note that we still have agent-to-agent interaction within the PDE domain during each time step, as the agents will be deleted based on their location at the end of the time step. This means that they can still contribute to transmission dynamics within that time window.

To facilitate the exchange between ABM and PDE in our hybrid model, the event data from the mobility dataset is sliced into chunks corresponding to individual time steps. Artificial events are introduced during this slicing to track the last known positions of all agents, allowing for consistent updates during each time step to exchange information between the models. For simplicity, we used the same strategy for the full-ABM, which may introduce some computational overhead. However, it offers the practical advantage of reduced memory usage by focusing only on the active time window. For visualization and boundary checking, each agent's exact position is calculated at the end of every time step.

2.4.1 Agent Enters PDE Domain

When an agent leaves the ABM domain and enters the PDE domain, the agent is removed from the ABM and their contribution is added to the PDE model. To do this, we project the agent's (continuous) spatial position onto the closest grid cell of the PDE mesh and increase the corresponding compartment density at that location. The amount added is the density equivalent of a single individual, which we precompute for each grid cell. This procedure ensures consistent mass transfer across the model boundary and preserves the total population in the hybrid model.

We assume that a single susceptible individual is to be added at a single grid point x^* , meaning that the density changes only at that specific location. This update is applied at the end of the time step, after the PDE solution has already been computed for all grid points x . We denote by $\tilde{S}(x, t_k)$ the PDE solution at time t_k before adding the contribution from agent transitions. With these assumptions, the following equation is satisfied, ensuring that the total added density corresponds to one individual:

$$\int_{\Omega_{Be}} S(x, t_k) - \tilde{S}(x, t_k) dx = 1,$$

which is equivalent to

$$\int_{\text{triangles touching } x^*} \varepsilon(x, t_k) dx = 1$$

since all other triangles of the grid are not affected, and ε denotes the density value equivalent to a single individual, which is to be determined. Further, we have

$$\int_{\text{triangles touching } x^*} \varepsilon(x, t_k) dx = \sum_{i=0}^{N_\Delta} \int_{\Delta_i} \varepsilon(x, t_k) dx \approx \sum_{i=0}^{N_\Delta} \frac{\varepsilon(x_1^i, t_k) + \varepsilon(x_2^i, t_k) + \varepsilon(x^*, t_k)}{3} \int_{\Delta_i} 1 dx,$$

where x_1^i, x_2^i, x^* denote the grid nodes of the triangle Δ_i and N_Δ is the total number of triangles touching the grid node x^* . Since we are only changing the density value at grid node x^* , we have $\varepsilon(x_1^i, t_k) = \varepsilon(x_2^i, t_k) = 0$ for $i = 0, \dots, N_\Delta$. Hence, we obtain

$$\frac{\varepsilon(x^*, t_k)}{3} \sum_{i=0}^{N_\Delta} |\Delta_i| \approx 1,$$

which leads to

$$\varepsilon(x^*) \approx \frac{3}{\sum_{i=0}^{N_\Delta} |\Delta_i|}.$$

2.4.2 PDE Person Enters Domain of ABM

To simulate agents transitioning from the PDE domain (Berlin) into the ABM domain (Brandenburg), we precompute the expected number of individuals present in the PDE model for each hour of the day. If the time step corresponds to one hour, this allows us to determine how many individuals should leave the PDE model and be represented as agents in the ABM.

The health status of the transitioning individuals is sampled based on the current distribution of the PDE compartment densities. To update the PDE densities, we first attempt to uniformly reduce the relevant compartments across all grid cells. If this leads to any density value becoming negative – which means that more individuals are removed than are available at certain locations – we switch to an alternative approach: We calculate the number of individuals that can be removed from each grid point, and store the corresponding grid indices. These indices are then shuffled, and a subset is randomly selected to determine the locations from which the transitions occur. The densities at the selected grid points are then reduced accordingly.

When an individual enters the ABM domain, we randomly pick a free agent ID, and the corresponding plan from the mobile phone-based event data is activated. This plan defines the agent’s activities and locations for the current day. Occasionally, the agent’s first or final position from that plan might be inside Berlin, i.e. outside of the ABM domain. These cases are not explicitly handled but occur infrequently in practice.

3 Parameter Identification

Finding optimal parameters for a stochastic ABM or a hybrid ABM–PDE model presents significant challenges due to the computational cost and variability inherent in such simulations. Several approaches have been proposed to address this issue. For instance, one may reduce the number of runs [23], rely on more efficient surrogate models to speed up optimization [4, 14, 25], reformulate the existing model to make parameter inference more tractable [18], adopt parameters from previous studies [22, 23] or even rely on manual parameter estimation [9]. In EpiSim, for example, parameters are fitted by minimizing the Root Mean Squared Logarithmic Error between the simulated and observed number of hospitalized cases [23]. Here, the authors use multiple (10 or 30) Monte Carlo runs and average the results to obtain stable estimates based on eight independent Monte Carlo seeds [23].

In our model, we used the previously optimized calibration parameter β_{const} for the infection rate for Berlin from the original EpiSim (see *BerlinSensitivityRuns.java* in [1]), adjusted by a factor to account for the changes in our implementation (see Sec. 4). The remaining parameters were taken from existing literature [22, 23]. For the Brandenburg model, we apply the same rates, since no region-specific calibration was available and the overall accuracy was sufficient for our focus on evaluating the coupling approach.

In contrast to the ABM, implementing the infection dynamics in the PDE model is more difficult, as the ABM’s infection process depends on numerous factors – such as shedding and intake rates, duration of interaction with infected agents, contact intensity, a calibration parameter corresponding to the infection rate in a compartmental model [22], and daily activity change rates – where some of these factors vary over time and across different facility categories. Translating these effects directly to the PDE model is challenging. One possibility is to only have the independent infection rate, which is constant with respect to time and fit it to target data.

Instead, we incorporate data that is applicable to all agents and for all categories, i.e., the activity change rates. For an ABM, implementing mild restrictions by considering changes in activity participation would alter agent trajectories and, consequently, the overall landscape. However, this change in landscape would likely not reduce infections but merely shift their locations. The implementation of activity reductions has the desired effect of reducing infection numbers, resulting, e.g., in a lower infection rate in the PDE system. For this reason, we directly incorporated changes in activity participation into the infection rate. We assume that a reduction in out-of-home activities corresponds to a decrease in infection numbers, and thus in the infection rate. Since this is an inverse relationship, we define the infection rate of the PDE model (3) as

$$\beta = \left(1 - \frac{\text{out-of-home activity change rate in \%}}{100\%} \right) \frac{\beta_{\text{const}}}{\pi r^2},$$

where β_{const} is the constant part of the infection rate that will be used for fitting and r is the contact radius (see Section 2.1.4). Since the contact radius is unknown, we determine it indirectly through the fitting of β_{const} , given that

$$\beta \pi r^2 = \left(1 - \frac{\text{out-of-home activity change rate in \%}}{100\%} \right) \beta_{\text{const}}.$$

For the ABM, we have the calibration parameter β_{const} corresponding to the infection rate in a compartmental model [22]. All final transition rates can be found in the next Section 4 in Tables 3 and 4.

School closures are handled differently, as they typically occur over a clearly defined time interval, leading to a more pronounced impact. Rather than scaling the infection rate or adjusting it to the changed landscape, we divide the simulation time interval into two phases – one without school closures and one with school closures – fitting the infection rates separately for these subintervals. In contrast, accounting for daily fluctuations in activity changes in the form of mild restrictions would require, fitting infection rates separately for each day, which is not feasible. Therefore, we directly incorporated these changes into the infection rate to account for their effects. Note that the constant part of the infection rate β_{const} is fitted separately for the PDE and ABM parts within the hybrid model, as their dynamics differ. The fitting is done using a simple grid search (see Sec. 4).

All other transition parameters are assumed to be the same across the ABM and PDE model. This is justified by the similarity of our trajectory-based ABM and the motion-based ABM (with landscape, see Section 2.1.1) from which the PDE is derived [14]. If Brandenburg were also modeled using PDEs, the same infection rate as in Berlin would be applied, consistent with the ABM design, where a single infection rate governs the entire spatial domain.

In principle, an ABM with simplified infection dynamics – and thus a correspondingly simplified hybrid model – could even serve as a reduced model for parameter inference, replacing the full-ABM in optimization loops. However, our focus in this paper lies not on optimal parameter fitting but on developing and evaluating a coupling mechanism between ABM and PDE approaches that can be applied to real-world data.

4 Implementation

The available mobile phone dataset contains event data for three distinct day types: weekdays, Saturday, and Sunday. This allows us to differentiate between typical mobility patterns across the week. We start our simulation on March 2, 2020, which is a Monday, and thus begin with weekday data. Agents are allowed to move beyond Brandenburg and Berlin, as the mobile phone data captures their locations across a wider region. These event-based trajectories are time-stamped and specify when an individual enters or leaves a facility of a certain type (e.g., home, work, leisure), allowing us to reconstruct realistic daily schedules.

In addition, we incorporate activity change rates to account for behavioral adaptations over time, such as reductions in out-of-home activities during the early phases of the pandemic. These rates also begin on March 2, 2020 (which matches the data provided in *be_2020mobility_data.csv* [5]), covering the period until June 12, 2020. The activity reductions are visualized in Figure 2 and are used to modulate infection dynamics in both the ABM and PDE components, as described in Section 2.2 for the ABM and in Section 3 for the PDE model. The first day assumes no reduction in activity participation and serves as a baseline.

The activity change rates represent relatively mild, day-specific restrictions in behavior. More substantial interventions – such as school closures – are considered starting from March 16, 2020. For simplicity and consistency in the simulation, we assume the same school closure date for both Berlin and Brandenburg, even though the actual dates differed slightly. According to [23], school closures in Berlin were implemented on March 16, 2020, while [30] mentions that most schools were closed on March 16, but the official closure was on March 17, 2020. In Brandenburg, [31] states that schools were officially closed on March 18, 2020.

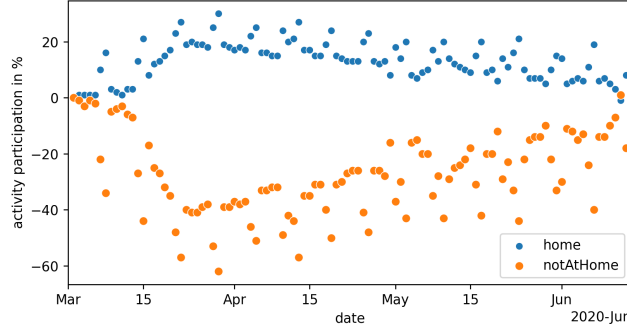


Fig. 2. Activity participation in % for activities at home and not at home including weekends.

Although mask-wearing has been implemented in the code, it was not required for the conducted experiments and thus has no effect on the presented results. In Berlin, mask mandates were introduced earlier in public transport (from April 27, 2020) and subsequently extended to public spaces such as shops on April 29, 2020 [30]. Since our model does not account for transmission in public transport, we defined April 28, 2020 as the final day of the simulation. From this point onward, a new modeling interval and a recalibration of the PDE infection rate would have been necessary.

To initialize the population distribution, we used the previously defined landscape (see equation (1)) to derive the initial distribution (see equation (4)). We visualized the process of landscape creation in the Appendix A. Figures 15 and 18 illustrate the distribution of agents for the 25% sample population and the full population, respectively. Figures 16 and 19 show the landscape of the agent distribution, including areas where no agent was ever present. In Figures 17a and 20a, these gaps were filled to prepare the data for the PDE model before transforming it to the triangular grid. Finally, Figures 17b and 20b display the landscape after the transformation.

The landscape, as defined in equation (1), depends on the diffusion coefficient. We computed the landscape and its gradient once and rescaled it according to changes in the diffusion coefficient. The gradient of the landscape is computed by first interpolating it from a rectangular grid (derived from the histogram of agent trajectories) to a triangular grid (used in the PDE model) using the `RegularGridInterpolator` from `scipy.interpolate`. The landscape is then defined for every grid node on the triangular grid. By incorporating information from the triangulation, which determines how grid points are connected by triangular elements, we create an object of the class `Triangulation` using `matplotlib.tri` and access its gradient using the `gradient` method.

The diffusion coefficient was selected to ensure limited individual movement over the short simulation period. We chose a value of $1e - 6$. The time step for simulation was set to half an hour ($1/48$ days), as we observed a significant improvement in accuracy compared to one-hour steps, with little further gain from finer time discretization.

For fitting the constant part of the infection rate in the PDE model (3), we used a simple grid search. We compared the mean absolute errors of five simulation runs against the target data for different parameter values. For the first time interval (March 2, 2020, to March 15, 2020), we initially tested $\beta_{\text{const}} \in \{3e + 2, 4e + 2, 5e + 2, 6e + 2\}$, while for the second time interval (March 16, 2020, to April 28, 2020), we considered $\beta_{\text{const}} \in \{1.1e + 2, 1.2e + 2, 1.3e + 2, 1.4e + 2, 1.5e + 2\}$ (see Table 1). We tested all combinations together, as the best choice for the first interval may minimize the error in that interval but could be far off for the second interval. The second interval begins with the implementation of school closures and is characterized by a significant change in the trajectory of the infection curve. The smallest errors were achieved with the parameters $5e + 2$ and $1.2e + 2$ (see Table 1). The parameter fitting for the scalar factor of the ABM infection rate was also performed using a simple grid search (see Table 2). All final transition rates can be found in Tables 3 and 4.

It is important to emphasize that the grid search was designed to be fast and coarse, sufficient for demonstrating the functionality of the hybrid model. Although the infection rate could be further optimized using more refined step sizes or advanced optimization methods, this was not the focus of our work. Since slight variations in these parameters do not significantly impact our overall conclusions, a more detailed optimization is beyond the scope of this paper.

The density values are checked to ensure they are non-negative at least once for each time step.

We created the modeling domain of Berlin using the boundary grid nodes of OpenDataLab [10]. The triangulation of the modeling domain Berlin was performed using `Triangle` [26], while the hybrid ABM-PDE systems were solved using the finite element method implemented in the `Kaskade7` software [13], with the `Dune` interface. For the coupling of the hybrid model, we use the `nanoflann` library [7] for efficient KD-tree construction in our implementation. Specifically,

		March 2, 2020 - March 15, 2020			
		$3e + 2$	$4e + 2$	$5e + 2$	$6e + 2$
March 16 - April 28, 2020	$1.1e + 2$	80.07	51.89	37.41	173.09
	$1.2e + 2$	76.23	47.85	29.37	188.09
	$1.3e + 2$	69.32	37.00	57.19	209.87
	$1.4e + 2$	67.02	31.83	103.78	263.99
	$1.5e + 2$	63.20	35.15	120.41	349.47

Table 1 Mean absolute error of the grid search (5 runs) for the hybrid model using a 25% population sample. The smallest error was achieved with the parameters $5e + 2$ and $1.2e + 2$.

March 2, 2020 - April 28, 2020			
$2.0 \cdot 1.7e - 5$	$2.2 \cdot 1.7e - 5$	$2.4 \cdot 1.7e - 5$	$2.6 \cdot 1.7e - 5$
42.59	41.25	41.39	47.63

Table 2 Mean absolute error of the grid search (5 runs) for the full-ABM using a 25% population sample. The smallest error was achieved with the parameter $2.2 \cdot 1.7e - 5$.

we use it to find the closest grid point to the position of an agent. The visualization of our simulation results was done using the `matplotlib` package in Python 3.9 and the grid was visualized using ParaView [27].

We computed the 7-day average of Covid-19 data from the RKI [16] and used it as our target data for parameter fitting, evaluation, and for our initial conditions. Our ABM is a streamlined version of EpiSim [1], implemented following [22, 23], with the exclusion of infection dynamics outside of facilities and without the use of weather data.

For computational reasons, previous studies such as [22] used a 25% sample of the full population and reported all results after scaling them to 100%. The 25% mobility dataset for Berlin is publicly available [5]. In our study, we do not use the Berlin data alone but rather the combined data for Brandenburg and Berlin, where the Berlin data is a subset of our dataset. It can be modified for independent tests or used to understand the data structure.

While prior work indicates that the outcomes of the 25% and 100% population models are largely similar, we explicitly examine both in this paper. Since the calibration parameter β_{const} was fitted to the 25% model, discrepancies are expected when applying it to the 100% model. In particular, the 100% model is likely to exhibit higher error, as no additional parameter optimization was performed. We measure both the average error and the average runtime to better understand the performance variations between the models. Particularly for the ABM and the hybrid model, we aim to assess how well the rates from the 25% model can be transferred to the 100% model. This will help determine whether parameter optimization can be performed using faster models and, for example, enable predictions for the entire population. Additionally, it will be interesting to compare whether the hybrid model with 100% of the population or the ABM with 25% of the population is faster, and which model potentially results in a lower error.

Implementing the model for 100% of the population results in changes to several data files. The event data file will be updated to include more people with events, the facility data file will expand to list additional facilities, and the maximum number of agents per facility in a given category will increase as more agents visit the same locations. Consequently, more facilities will be included overall. In [22, 23], it was mentioned that $N^{\text{spacesPerFacility}}$ needs to be adjusted for the entire population. However, we will not modify this parameter, as other factors, such as room size, will also change, effectively counteracting the need to scale $N^{\text{spacesPerFacility}}$. The calibration parameter β_{const} will remain unchanged. The infection rate in the ABM depends on multiple factors, with contact intensity being the most affected. This is primarily due to changes in the maximum number of agents per facility within a given category when adjusting the dataset size.

It is worth noting that the infection rate in the ABM depends on multiple factors. Among them, contact intensity is most affected by scaling, since the number of agents per facility changes with dataset size. The infection rate β in the PDE model, however, must be explicitly rescaled. This is due to its nonlinear structure: it includes terms that represent pairwise interactions (e.g., between susceptibles and infectious), which scale quadratically with population size. In contrast, the other transition rates represent individual-level processes and remain unchanged.

While infections in the simulation occur across various locations and times, official case data reported by the Robert Koch Institute (RKI) are aggregated by the main residence of infected individuals, in accordance with § 11 of the Infection Protection Act (IfSG)². Therefore, to match simulation results with reported data, we sum the number of

²https://www.gesetze-im-internet.de/ifsg/_11.html

	from March 2, 2020	from March 16, 2020	March 2, 2020 - April 28, 2020								
	β_{const}	β_{const}	σ	γ	η	κ	η_c	ϕ_i	ϕ_{sy}	ϕ_h	ϕ_{hc}
full-ABM	$2.2 \cdot 1.7e - 5$	$2.2 \cdot 1.7e - 5$	$1/3.5$	$1/2$	$1/4$	1	$1/21$	$1/4$	$1/8$	$1/14$	$1/7$
hybrid	$5e + 2$	$1.2e + 2$	$1/3.5$	$1/2$	$1/4$	1	$1/21$	$1/4$	$1/8$	$1/14$	$1/7$

Table 3 Transition rates of the full-ABM and hybrid model using a 25% population sample.

	from March 2, 2020	from March 16, 2020	March 2, 2020 - April 28, 2020								
	β_{const}	β_{const}	σ	γ	η	κ	η_c	ϕ_i	ϕ_{sy}	ϕ_h	ϕ_{hc}
full-ABM	$2.2 \cdot 1.7e - 5$	$2.2 \cdot 1.7e - 5$	$1/3.5$	$1/2$	$1/4$	1	$1/21$	$1/4$	$1/8$	$1/14$	$1/7$
hybrid	$1.25e + 2$	$3e + 1$	$1/3.5$	$1/2$	$1/4$	1	$1/21$	$1/4$	$1/8$	$1/14$	$1/7$

Table 4 Transition rates of the full-ABM and hybrid model for the full population (100%).

symptomatic individuals in the simulation across all locations. However, this may lead to overestimation, as our model includes individuals who live outside Berlin and Brandenburg but were present in the simulation domain.

Tracking the health status of each agent across simulation days requires identifying agent IDs. This is feasible in the ABM but not in the PDE contribution of the hybrid model, where no agent IDs exist. As a result, some information is inevitably lost in the hybrid setting. For instance, if a recovered individual enters the PDE domain and later reappears in the ABM, they may be reinitialized as susceptible. This does not align with our health state transitions and highlights a key limitation of our hybrid model, which combines compartment densities with individual-level agents (see Section 2.1.2).

5 Numerical Results

In this section, we present the numerical results of our simulations for both the pure ABM and the hybrid model, which integrates both agent-based and PDE-based components. We begin in Section 5.1 by describing the spatial discretization used for the PDE domain, including the grid construction and its key properties. Next, in Section 5.2, we will discuss the number of simulation runs and evaluate performance in terms of runtime and error metrics. In Section 5.3, we compare the computational efficiency and accuracy of the ABM and hybrid model, highlighting the trade-offs introduced by coupling the two approaches. Finally, Section 5.4 presents a set of extreme-case experiments designed to test the robustness and behavior of the hybrid model under challenging conditions. All experiments are conducted for two different population scenarios: a 25% sample of the full dataset, with results scaled accordingly, and the complete 100% population.

5.1 Grid

We created a coarse grid of Berlin's modeling domain (see Fig. 3). The mesh can be constructed via

```
triangle -pqa750000.0 <general name of poly file without ending>
```

for a mesh setup consisting of 1,884 triangles, 1,053 nodes and 179 boundary nodes. The -p switch loads a .poly file, which can define points, segments, holes, regional attributes, and area constraints (see *Command line switches* in [26]). With the -q switch, vertices are added to the mesh to ensure that no angle smaller than 20° occurs. Using the -a switch, along with the value 750000.0, imposes a maximum triangle area of 750000.0. Finally, the -p switch will generate a conforming constrained Delaunay triangulation, provided that either the -q or -a switch is also used.

5.2 Number of Runs

We will visualize the plots to observe when the cumulative runs stabilize and how finely the y-values are chosen. By applying specific thresholds for the relative changes between neighboring cumulative runs, we will analyze in detail how many runs are needed to reach the desired threshold for both the full-ABM and the hybrid model, for 25% and 100% of the population. This will be assessed in terms of both error and duration, with separate evaluations for each.

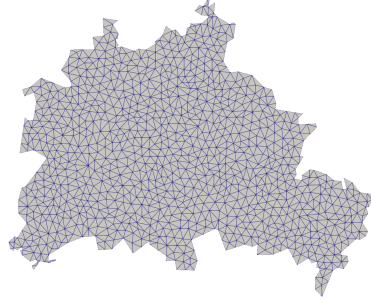


Fig. 3. Modeling domain of PDE contribution (3) of hybrid model.

5.2.1 25% Population

Figs. 4a and 4b show the cumulative absolute mean error of the ABM and hybrid model, respectively, based on 100 runs using a 25% population sample. The relative difference between consecutive values is used as a threshold to determine

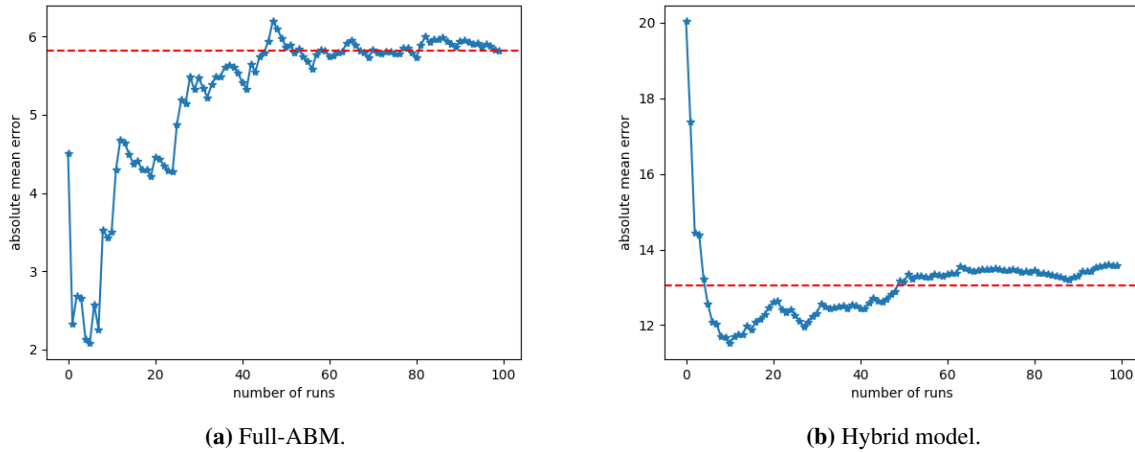


Fig. 4. Cumulative absolute mean error of 100 runs using a 25% population sample. Red line is mean of all cumulative runs.

the necessary number of runs. With a 1% relative difference between consecutive values, the hybrid model requires 29 runs, while the full-ABM requires 92 runs. Beyond 92 runs, the difference between consecutive values remains below 1%, meaning additional runs (e.g., 93) do not significantly impact the result. This results in a 64-run reduction for the hybrid model.

For a 0.5% relative difference, the hybrid model requires 54 runs, whereas the full-ABM needs 100 runs, leading to a 46-run reduction for the hybrid model.

Thus, halving the threshold roughly doubles the required runs for the hybrid model. Since the hybrid model already requires fewer runs than the full-ABM, this difference remains significant even for stricter thresholds, maintaining a substantial reduction in computational effort.

Computational time must be measured over multiple runs, as it can vary significantly depending on several factors. For example, the duration of individual disease courses can be highly variable. Additionally, reductions in activity participation can impact transmission dynamics by limiting interaction opportunities, potentially altering the computational load. By averaging across multiple runs, we ensure a more reliable estimate of computational time that accounts for these fluctuations.

The cumulative mean running times of 10 runs are displayed in Figs. 5a and 5b for the full-ABM and the hybrid model, respectively. The hybrid model achieves a threshold of 0.05% within the first two runs, whereas the ABM is initially close to 0.12%. For a threshold of 0.02%, the hybrid model achieves this again within two runs, while the ABM requires 10 runs. The hybrid model reaches 0.01% after just 9 runs, whereas the ABM's relative difference between the last two cumulative runs remains around 0.016%.

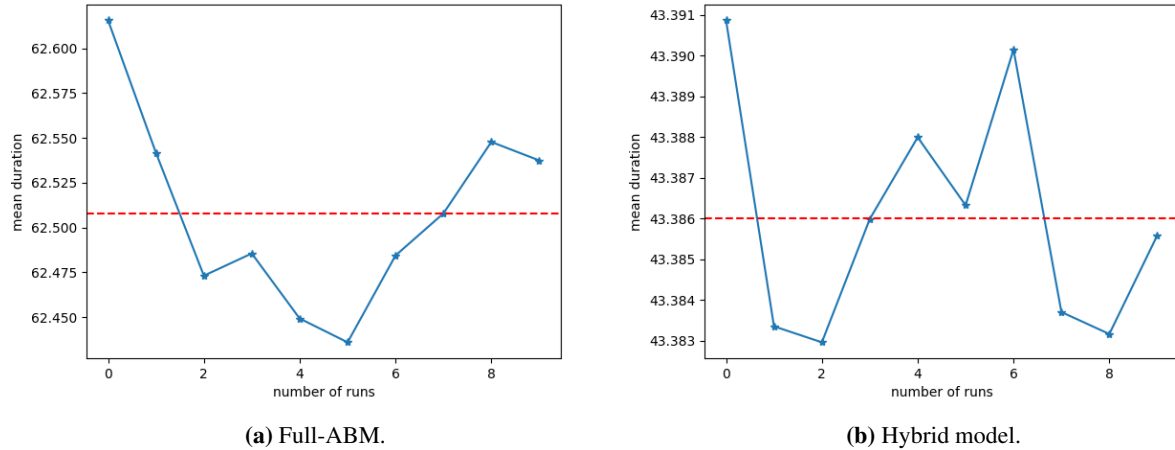


Fig. 5. Cumulative mean running times of 10 runs using a 25% population sample. Red line is mean of all cumulative runs.

5.2.2 100% Population

The cumulative absolute mean error for the ABM and hybrid model, based on 100 runs with the full population sample (100%), is shown in Figs. 6a and 6b, respectively. With a 1% relative difference between consecutive values, the hybrid model requires 28 runs, whereas the full-ABM only needs 10. Beyond this point, additional runs (e.g., 11) have little effect, as the relative difference remains below 1%, resulting in an 18-run reduction for the full-ABM.

For a 0.5% relative difference, the hybrid model requires 64 runs, while the full-ABM needs only 30, leading to a 34-run reduction for the full-ABM. Notably, when the threshold is halved, the hybrid model requires about twice as many runs, whereas the ABM's run count triples. Despite requiring fewer runs, the ABM now shows a clear advantage over the hybrid model, as it remains significantly more efficient in this setting.

We observe a significant decrease in the number of runs required for the ABM when increasing the population from a 25% sample to the full population. Assuming that the ABM for the full population takes four times longer to run than for the partial population, the choice of which sample to use depends on the selected threshold in combination with the number of runs and the hypothetical duration of a single run. For a threshold of 1%, using the full population is clearly more efficient, whereas for a threshold of 0.5%, the smaller sample proves to be the better option.

Interestingly, when examining the hybrid model results, the number of runs required for the full population either increases or remains almost the same compared to the partial sample. In contrast, the ABM shows a noticeable decrease in the required number of runs. Regardless of the chosen threshold, this means that the hybrid model with the smaller population sample is, overall, probably the better choice for saving total simulation time to achieve stable results, assuming that the model for the full population will be slower than for the partial sample. For a proper efficiency comparison between the hybrid model and the ABM, the exact running times per single run are required.

Figs. 7a and 7b present the cumulative mean running times over 10 runs for the full-ABM and hybrid model, respectively. Again, the hybrid model achieves a threshold of 0.05% with only the first two runs. In contrast, the ABM is close to 0.7%. For a 0.02% relative difference, the hybrid model reaches the threshold with the first two runs, while the ABM requires more than 10 runs.

For a 0.01% relative difference, the hybrid model achieves the desired threshold with just 10 runs. Specifically, the relative difference between the first two cumulative runs is 0.0121%. In contrast, the ABM requires more than 10 runs, with the relative change between the last consecutive runs being 0.0431%.

5.3 Computational Time vs. Accuracy

Next, we will compare computational time and accuracy of both models for both population sizes. Although Section 5.2 demonstrated that the hybrid model requires fewer runs than the full-ABM for the same threshold, we still evaluate 100 runs for all models. Since these runs were already generated in the previous experiment, we simply reuse them for this analysis. We assess accuracy based on the mean and standard deviation over all runs, with values plotted up to the final time $T = 58$, while the overall mean across the entire time period for all runs is reported. Additionally,

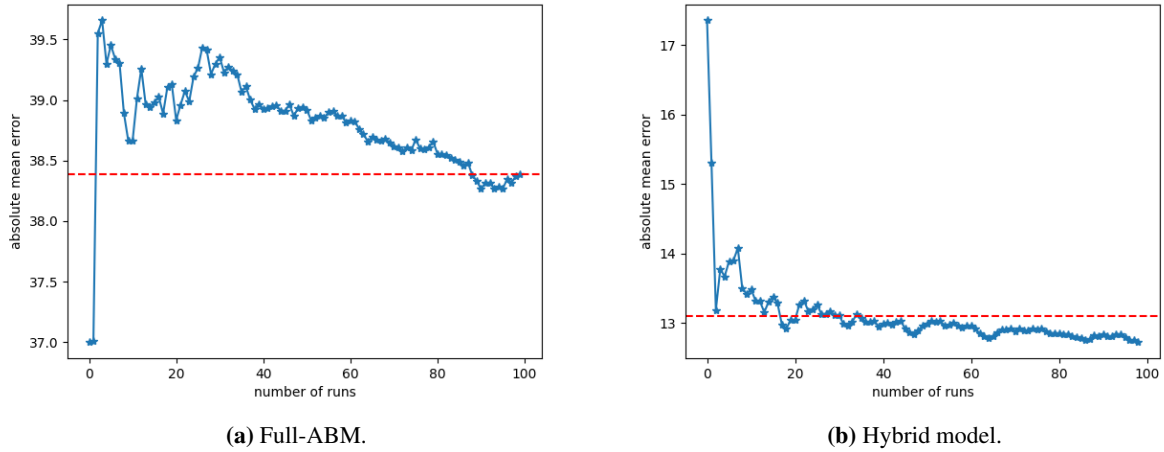


Fig. 6. Cumulative absolute mean error of 100 runs using the full population sample (100%). Red line is mean of all cumulative runs.

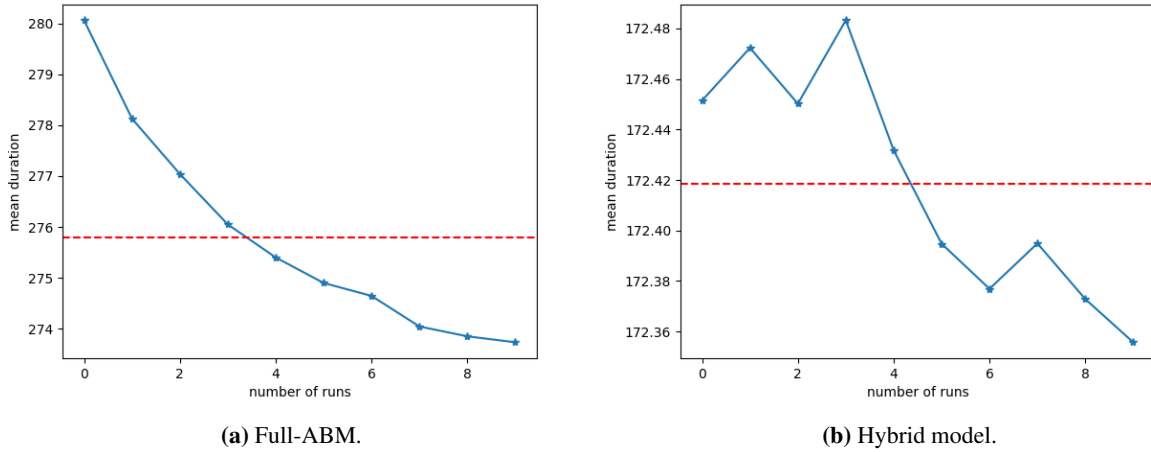


Fig. 7. Cumulative mean running times of 10 runs using the full population sample (100%). Red line is mean of all cumulative runs.

we measure the change in accuracy and computational time from the full-ABM to the hybrid model using the relative difference in their mean values, given by

$$\frac{\mu_{\text{hybrid}} - \mu_{\text{full-ABM}}}{\mu_{\text{full-ABM}}},$$

where μ_{hybrid} and $\mu_{\text{full-ABM}}$ denote the (absolute) mean values of the hybrid and full-ABM models, respectively. Computational time was measured with the parameter setting `verbosity=0` in the `covid.cpp` file, which reduces print outputs, prevents the creation of plots, disables the saving of agent health state and location data, and avoids storing density-related information.

5.3.1 25% Population

The fitted results of the hybrid model and the full-ABM, along with their target data, can be observed in Figs. 8a and 8b, respectively. The results represent the mean over 100 runs, with the corresponding standard deviation shown in the figures. The results for the error of the full-ABM and hybrid model are shown in Table 5, while the duration for both models is presented in Table 6. Unlike in the original paper [23], the error was not measured logarithmically. The error of the hybrid model is likely lower than that of the ABM due to the separate fitting of the two time intervals. However, this does not guarantee that the same holds for other federal states or subregions in general, nor for longer time intervals. Furthermore, if the time interval is not split, there is no guarantee that the error of the hybrid model will remain lower.

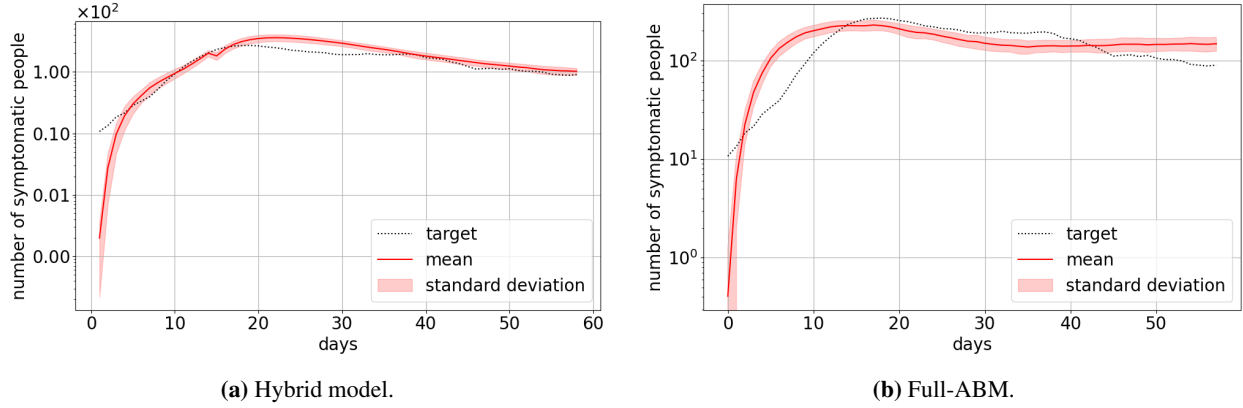


Fig. 8. Mean and standard deviation of the number of symptomatic individuals and target values for a 25% population sample in Berlin-Brandenburg (100 runs).

It is also important to note that the parameter optimization was conducted in a coarse manner, and better results could potentially be achieved for both the ABM and the hybrid model.

Since the infection dynamics in the PDE model are only varied by activity data and fewer direct data are used compared to the ABM, the PDE model – and thus the hybrid model – may be less suitable for predictions when compared to the ABM. However, the advantage of the hybrid model with its lower error is that we achieved a very good fit using the same compartments as the ABM, but with less complex infection dynamics, all while conducting a fast and rough parameter fitting.

	full-ABM	hybrid
absolute mean error to target	42.56	37.81
increased error to previous model	-	-11.16%

Table 5 Error of the full-ABM and hybrid model (100 runs) using a 25% population sample.

	full-ABM	hybrid
mean duration in min.	62.54	43.39
decreased duration to previous model	-	30.62%

Table 6 Duration of the full-ABM and hybrid model (10 runs) using a 25% population sample.

5.3.2 100% Population

The fitted results for the hybrid model and the full-ABM, along with their corresponding target data, are shown in Figs. 9a and 9b, respectively. Again, these results represent the mean across 100 simulation runs, with the associated standard deviation displayed in the figures. The error results for the full-ABM and hybrid model are presented in Table 7, while the runtime for both models is shown in Table 8. The fitting was performed using the 25% population dataset, so we expected higher errors when applying it to the full population dataset. However, this is only the case for the ABM, while the hybrid model does not exhibit a higher error. Hence, the increased error compared to the previous model went from -11.16% to -51.25%.

The runtime of the hybrid model has almost quadrupled, while the runtime of the ABM has increased by more than a factor of four. As a result, the decreased duration compared to the previous model rises from 30.62% to 37.06%.

	full-ABM	hybrid
absolute mean error to target	52.70	25.69
increased error to previous model	-	-51.25%

Table 7 Error of the full-ABM and hybrid model (100 runs) using the full population sample (100%).

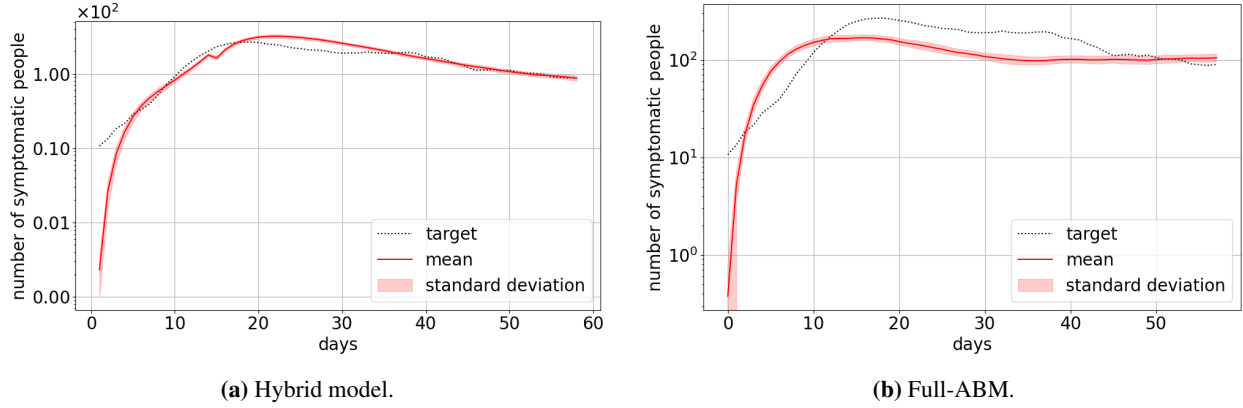


Fig. 9. Mean and standard deviation of the number of symptomatic individuals and target values for the full population sample (100%) in Berlin-Brandenburg (100 runs).

	full-ABM	hybrid
mean duration in min.	273.85	172.36
decreased duration to previous model	-	37.06%

Table 8 Duration of the full-ABM and hybrid model (10 runs) using the full population sample (100%).

Now, knowing the least number of runs needed for both thresholds (1% and 0.5%), as well as the runtime for a single run, we can conclude that the total simulation time of the hybrid model for the partial sample is the smallest, requiring at least 20.97 hours for the 1% threshold and 39.05 hours for the 0.5% threshold. In the case of the ABM, it depends on the chosen threshold. For the 1% threshold, the full population sample should be used, which requires a total simulation time of at least 45.64 hours. For the 0.5% threshold, the partial population sample should be used, which requires a total simulation time of at least 87.83 hours.

5.4 Extreme Cases

To test whether the coupling works in both directions and to evaluate the model's stability, we will conduct experiments for extreme cases. People continue to follow their daily activities, and restrictions are imposed as before. The only change we make is to the initial health state of all individuals. All agents are initially exposed and therefore soon become infectious, while the PDE population is initially susceptible, and vice versa. In these experiments, we can observe the influence of commuting individuals from Berlin or Brandenburg on each other's infection dynamics.

The agents' locations are plotted with their respective health states using different colors: **susceptible**, **exposed**, **infectious**, **symptomatic**, **requires hospitalization**, **critical**, **removed**.

5.4.1 25% Population

The total number of symptomatic individuals for the ABM contribution and the PDE contribution (3) of the hybrid model are shown in Figs. 10a and 11a, while snapshots of the corresponding experiments can be found next to these plots in Figs. 10b and 11b. For better comparability, we set the maximum of the y-axis to the same value in the total number plots.

Examining the total number of plots, we observe a significant difference in how the states influence each other. In the first experiment (see Fig. 10a), the peak number of symptomatic individuals in Berlin (blue) is significantly higher than in Brandenburg, to the extent that the small wave in Brandenburg is barely visible. In the second experiment (see Fig. 11a), the peaks have shifted toward each other: the peak in Berlin is lower than in the first experiment, while the peak in Brandenburg is now clearly visible. However, the peak in Brandenburg remains significantly lower than the previous peak in Berlin from the first experiment. It is evident that there is a notable difference depending on which model the entire population is set to exposed or susceptible.

Additionally, we observe the formation of a second wave in Brandenburg in the second experiment, with a sharp decline followed by a significant increase in symptomatic cases between the waves. However, upon closer inspection of the data (see Fig. 10a), this pattern is also present in the first experiment in the ABM, where a small second wave, if we

may call it that, forms in a similar manner. The increases and decreases in the first experiment in the ABM, where we observe very few cases, seem to be partially driven by the activity data (see Fig. 2). However, this is less the case for the other scenarios, where the waves are more pronounced, and the symptomatic cases are significant. Nevertheless, it is possible that the activity data triggered the formation of the second wave. Interestingly, in the first experiment for the ABM, the number of symptomatic cases even reaches 0.0 between the waves.

The peak in Berlin occurs on day 18, shortly after the second time interval with the lower infection rate begins. It is worth noting that the activity change rates, together with the increasing cases in Berlin, may have contributed to the formation of a second wave. After adjusting the implementation to prevent individuals from jumping out of the PDE domain into the ABM (see Fig. 12), a second wave is still visible, and it appears almost identical in the case of the ABM compared to the previous experiment with full coupling. Hence, the influence of Berlin is small or not clearly visible in this case. Additionally, as the individuals in the PDE domain are required to stay in Berlin, symptomatic cases have slightly increased in Berlin.

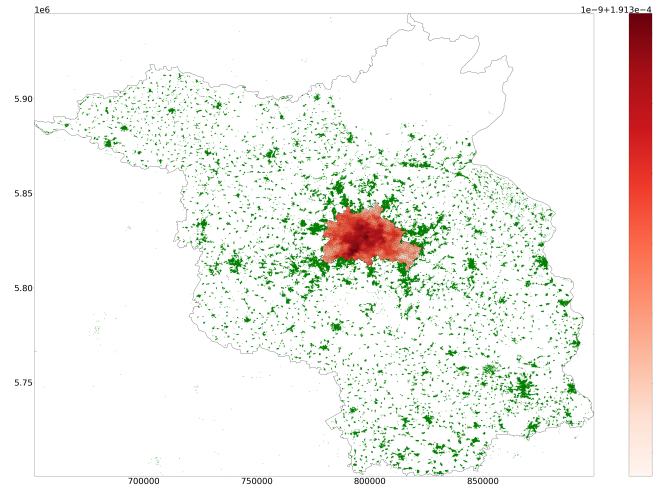
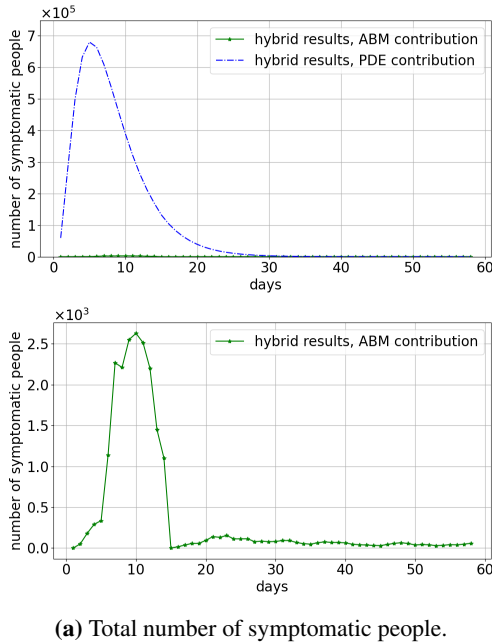


Fig. 10. Everyone in PDE model contribution (3) of hybrid model is initially exposed and everyone in ABM contribution of hybrid model is initially susceptible.

5.4.2 100% Population

Similarly, the total number of symptomatic individuals for the ABM and PDE contributions (3) of the hybrid model are presented in Figs. 13a and 14a. Corresponding experiment snapshots are displayed next to these plots in Figs. 13b and 14b. Again, to ensure comparability, the y-axis maximum has been set to the same value across the total number plots.

The upper plot in Fig. 13a appears identical to the upper plot in Fig. 10a, whereas the lower plot closely resembles the lower plot in Fig. 10a. The peak of the ABM curve is higher for the partial population, but it is important to note that this result is based on a single run. Once again, the increases and decreases, particularly in the first experiment within the ABM, appear to be partially driven by the activity data (see Fig. 2).

Looking at the total numbers plot of the second experiment (see Fig. 14a), it appears similar to the plot for the 25% population sample (see Fig. 11a). Indeed, both plots are quite similar, with a slightly higher overall number of symptomatic individuals. Notably, both peaks are somewhat higher but occur on the same days.

6 Discussion

Our hybrid modeling approach, which integrates an agent-based model (ABM) with a partial differential equation (PDE) model, offers several advantages but also introduces new challenges. A key limitation lies in the deterministic nature of the PDE component, meaning that, e.g., variability in disease duration and the effect of fluctuating contact opportunities

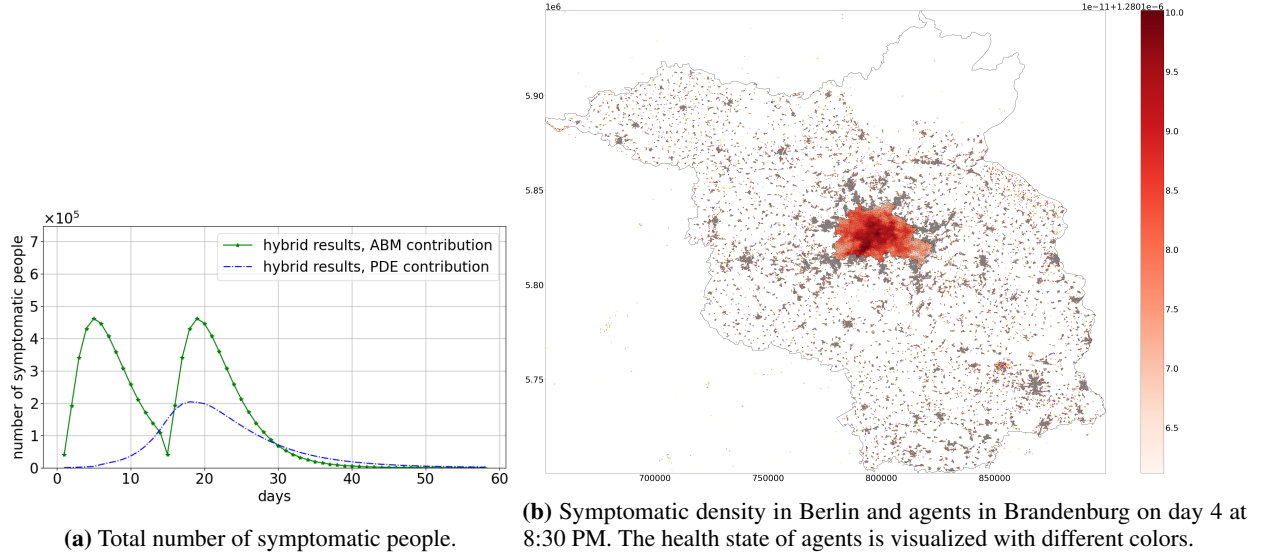


Fig. 11. Everyone in ABM contribution of hybrid model is initially exposed and everyone in PDE model contribution (3) of hybrid model is initially susceptible. A 25% population sample is used.

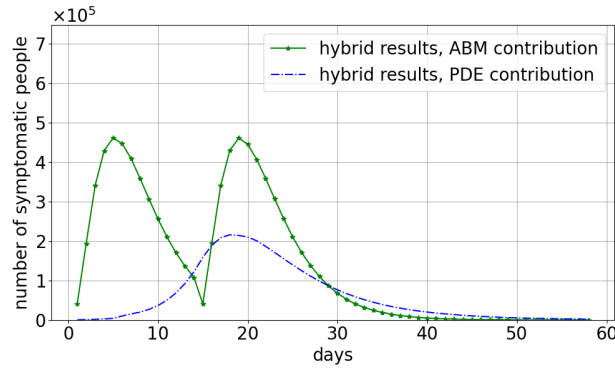
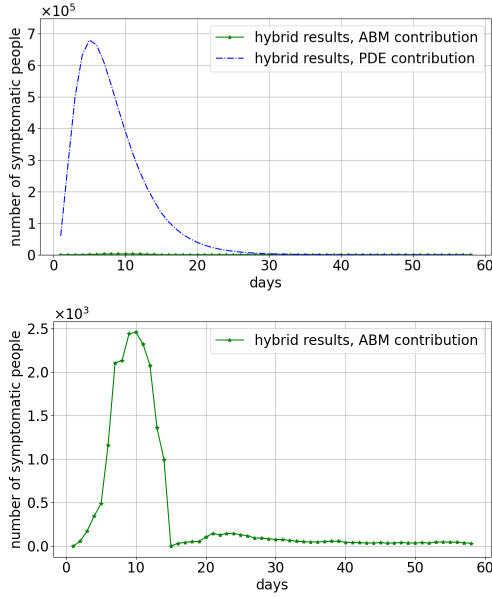


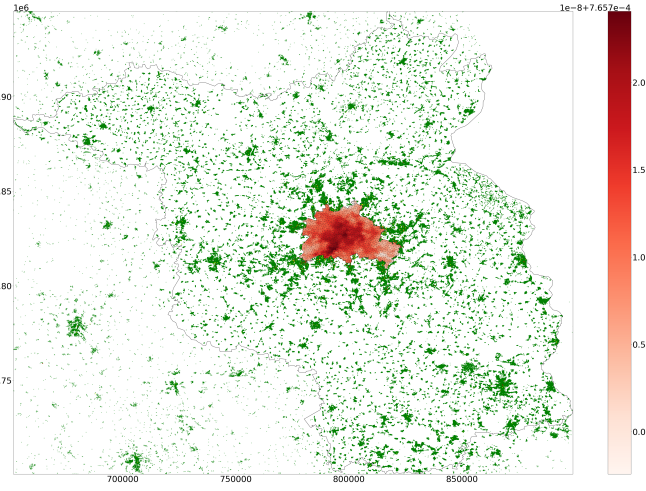
Fig. 12. Total number of symptomatic people. Everyone in ABM contribution of hybrid model is initially exposed and everyone in PDE model contribution (3) of hybrid model is initially susceptible. The jumping of agents from the PDE domain to the ABM domain has been removed.

on transmission dynamics are not present in this part of the model. On the other hand, the hybrid coupling introduces new sources of variability through information loss, such as a recovered agent entering Berlin and later reappearing as a susceptible agent, which introduces changes to the theoretical dynamics (see Fig. 1), which may increase variance. As we scale the 25% population results to the full population, the variance will scale accordingly, resulting in a larger variance for the scaled 25% population results. Additionally, changing the population size affects the maximum number of agents present in a facility of a given category. For the full population, this number is higher for the same facility compared to the partial sample. As a result, the probability of infection decreases when the same number of people are inside the facility. This lower probability of infection may contribute to a lower overall variance. When considering the total population, the probability of infection fluctuates less when an infectious agent leaves a facility compared to the partial population sample, making the changes less drastic. At the same time, incorporating more people into the model increases mixing. Given the complexity of these effects, the most reliable approach was to conduct simulations.

The deterministic PDE dynamics and the coupling process both reduce variability in the 25% scenario, but this effect does not hold for the full population. In fact, the hybrid model introduces a different type of noise due to the abstraction and simplification of agent-level dynamics. Agent identifiers are lost in the PDE region, leading to mismatches when assigning states upon re-entry to the ABM. For instance, an agent may reappear earlier or later than expected, or with an incorrect health status. To mitigate this, we propose future improvements such as storing metadata when an agent transitions into the PDE domain – including expected return time and current health status. Upon re-entry, this information could be used to assign a health state based on time spent in the PDE region and the transition dynamics

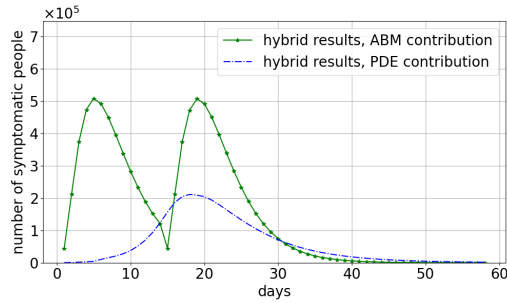


(a) Total number of symptomatic people.

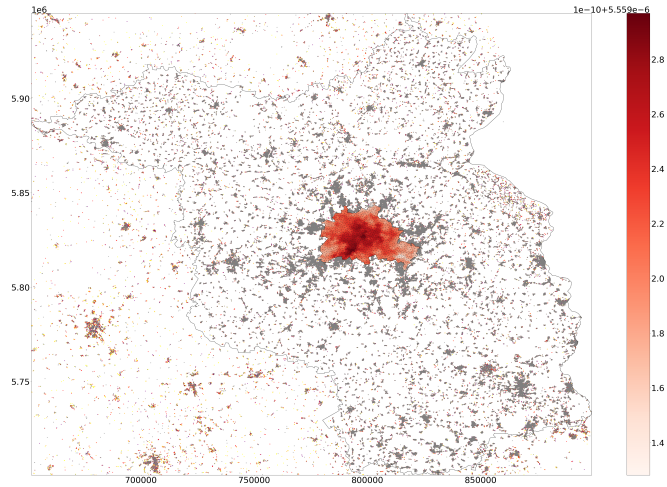


(b) Symptomatic density in Berlin and agents in Brandenburg on day 4 at 4:30 PM. The health state of agents is visualized with different colors. The full population sample (100%) is used.

Fig. 13. Everyone in PDE model contribution (3) of hybrid model is initially exposed and everyone in ABM contribution of hybrid model is initially susceptible.



(a) Total number of symptomatic people.



(b) Symptomatic density in Berlin and agents in Brandenburg on day 4 at 8:30 PM. The health state of agents is visualized with different colors. The full population sample (100%) is used.

Fig. 14. Everyone in ABM contribution of hybrid model is initially exposed and everyone in PDE model contribution (3) of hybrid model is initially susceptible. The full population sample (100%) is used.

from the compartment model (see Fig. 1). This strategy would help reduce artificial variance introduced by random reassignment. Additionally, stochasticity could be reintroduced into the PDE model itself – for example, through noise terms in the compartment equations – to better reflect variability in transitions.

We used a 25% sample of the full dataset, which is also employed for calibration and evaluation in existing studies [22, 23]. For readers interested in population sampling strategies, we refer to the general context of population sampling [2, 3] and in the context of mobility ABMs [6, 29].

Interestingly, while the number of cases in Berlin has little influence on the infection wave in Brandenburg, there is a strong influence in the other direction. This asymmetry is especially visible in our plots when varying the population size, for example, in Figs. 10a and 13a, but especially through the extreme experiments within the same population

size. It is important to keep in mind that the population size in Berlin is significantly larger than in Brandenburg and also larger than the total number of agents in the ABM contribution of the hybrid model. One explanation lies in the asymmetry of commuting: according to data from 2021, around 270,000 inhabitants of Brandenburg had their work place in Berlin, while only around 108,000 inhabitants of Berlin had their work place in Brandenburg [12]. These numbers likely underestimate the actual pre-pandemic commuting flows due to increased remote work in 2021. Still, they highlight the significant directional influence of Brandenburg on Berlin.

From a technical perspective, there are several opportunities for performance improvements, e.g., for better runtime and better memory efficiency. For instance, the ABM was not implemented in the most efficient way but rather in the same manner as the ABM component of the hybrid model. The hybrid model itself also offers room for optimization, such as interrupting the ABM event data evaluation to perform a PDE step and exchange information between both models. This would allow the use of the entire event dataset instead of creating and working with sliced event data, as done in this paper. Rather than creating artificial event slices, a more efficient approach could be to store the index of the last evaluated event for each agent and compute their position inside a facility at the beginning of each time step during runtime. Additionally, by pre-labeling facilities within the PDE region, it would be possible to determine more quickly whether an agent is entering the PDE region. If an agent is commuting, a lookup could be performed to check whether the transition is from a facility to the PDE region, allowing for a faster decision on whether a jumping process should occur. The precise implementation details still need to be determined.

7 Conclusion

In this paper, we presented a novel hybrid modeling approach that couples agent-based models (ABMs) with partial differential equations (PDEs) to efficiently simulate epidemiological dynamics across heterogeneous geographic regions. Our approach leverages the individual-level detail of ABMs while incorporating the spatially continuous representation of PDEs, allowing for a more computationally efficient yet spatially resolved simulation framework. Our results demonstrate how the integration of these two components improves model efficiency and highlights its ability to capture key epidemiological dynamics, such as commuting-driven transmission between Berlin and Brandenburg.

By applying this hybrid ABM-PDE model to the Berlin-Brandenburg region using real-world mobility and infection data, we demonstrated its ability to capture the distinct epidemiological dynamics of urban and rural areas. The model successfully reduced computational cost significantly compared to a full-ABM simulation. This efficiency gain becomes evident when comparing the simulation times and error margins of the hybrid model and the full-ABM. Specifically, the hybrid model achieved shorter simulation times and lower errors than the ABM, regardless of whether a partial (25%) or full (100%) population sample was used. Thus, our hybrid approach is a practical alternative for real-time epidemiological assessments. A key advantage over full-ABM models such as EpiSim is that our approach allows for efficient simulations of 100% of the population on a standard laptop, making large-scale epidemiological modeling more accessible and computationally feasible.

Looking ahead, we aim to extend this hybrid framework into a fully integrated ABM-PDE-ODE system, allowing for even more flexible and modular modeling of complex disease dynamics across varying spatial and structural scales.

Acknowledgments

We acknowledge Kai Nagel for valuable discussions on the agent-based model. We also thank Jakob Benjamin Rehmann and Sydney Cornelia Paltra for providing essential data for the Berlin and Brandenburg experiments and for assistance with their software. We would like to thank Inan Bostanci for the many meetings and constructive feedback throughout the process.

The work on this paper was funded by the German Ministry of research and education (BMBF) (project ID: 01KX2022A) and by the Deutsche Forschungsgemeinschaft (DFG, German Research Foundation) under Germany's Excellence Strategy via MATH+: The Berlin Mathematics Research Center (EXC-2046/1, project ID: 390685689).

References

- [1] Public github repository “matsim-episim-libs”. <https://github.com/matsim-org/matsim-episim-libs>.
- [2] Sirwan Khalid Ahmed. How to choose a sampling technique and determine sample size for research: A simplified guide for researchers. *Oral Oncology Reports*, 12:100662, 2024.
- [3] Mohammad Daud Ali and Ebrahim Ahmed Jaber Al Hatf. Types of sampling and sample size determination in health and social science research. *Journal of Young Pharmacists*, 16(2):204–215, June 2024.
- [4] Claudio Angione, Eric Silverman, and Elisabeth Yaneske. Using machine learning as a surrogate model for agent-based simulations. *PLOS ONE*, 17(2):1–24, 02 2022.
- [5] Michael Balmer, Ricardo Ewert, Sebastian Alexander Müller, Kai Nagel, Andreas Neumann, and Christian Rakow. Synthetic activity chains for agent-based epidemiological simulations of Berlin. Version 2, DepositOnce, TU Berlin, 2022. Accessed: 2025-03-11. <https://doi.org/10.14279/depositonce-11495.2>.
- [6] Federico Bigi, Taha Hossein Rashidi, and Francesco Viti. Synthetic population: A reliable framework for analysis for agent-based modeling in mobility. *Transportation Research Record*, 2678(11):1–15, 2024.
- [7] Jose Luis Blanco and Pranjal Kumar Rai. nanoflann: a C++ header-only fork of FLANN, a library for nearest neighbor (NN) with kd-trees. <https://github.com/jlblancoc/nanoflann>, 2014.
- [8] Inan Bostanci and Tim Conrad. Integrating agent-based and compartmental models for infectious disease modeling: A novel hybrid approach. *Journal of Artificial Societies and Social Simulation*, 28(1):5, 2025.
- [9] Dipanjan Chakraborty, Saikat Batabyal, and Vitaly V. Ganusov. A brief overview of mathematical modeling of the within-host dynamics of mycobacterium tuberculosis. *Frontiers in Applied Mathematics and Statistics*, 10, 2024.
- [10] Adrian Stabiszewski Felix Ebert. Geojson utilities. <https://opendatalab.de/projects/geojson-utilities/>, 2018. Created by OpenDataLab. Accessed: 2025-02-13.
- [11] Félix Foutel-Rodier, François Blanquart, Philibert Courau, Peter Czuppon, Jean-Jil Duchamps, Jasmine Gamblin, Élise Kerdoncuff, Rob Kulathinal, Léo Régnier, Laura Vuduc, et al. From individual-based epidemic models to mckendrick-von foerster pdes: A guide to modeling and inferring covid-19 dynamics. *Journal of Mathematical Biology*, 85(4):43, 2022.
- [12] Amt für Statistik Berlin-Brandenburg. Neuer pendleratlas für deutschland: Eine million menschen pendelten 2021 in der hauptstadtregion, November 2022. Pressemitteilung Nr. 250, Accessed: 2025-03-12. <https://www.statistik-berlin-brandenburg.de/250-2022>.
- [13] S. Götschel, A. Schiela, and M. Weiser. Kaskade 7 – a flexible finite element toolbox. *Comp. Math. Appl.*, 81:444–458, 2020.
- [14] Luzie Helfmann, Nataša Djurdjevac Conrad, Ana Djurdjevac, Stefanie Winkelmann, and Christof Schütte. From interacting agents to density-based modeling with stochastic pdes. *Communications in Applied Mathematics and Computational Science*, 16(1):1–32, January 2021.
- [15] N. Juhász, F. A. Bartha, S. Marzban, R. Han, and G. Röst. Probability of early infection extinction depends linearly on the virus clearance rate. *Royal Society Open Science*, 11(10):240903, 2024.
- [16] Robert Koch-Institut. Sars-cov-2 infektionen in deutschland. Data set, Zenodo, 2025. Accessed: 2024-11-19. <https://doi.org/10.5281/zenodo.15004660>.
- [17] Margarita Kostre, Christof Schütte, Frank Noé, and Mauricio del Razo. Coupling particle-based reaction-diffusion simulations with reservoirs mediated by reaction-diffusion pdes. *Multiscale Modeling & Simulation*, 19:1659–1683, 11 2021.
- [18] Jacopo Lenti, Fabrizio Silvestri, and Gianmarco De Francisci Morales. Variational inference of parameters in opinion dynamics models. *CoRR*, abs/2403.05358, 2024.
- [19] De-Zhang Li and Xiao-Bao Yang. On numerical stationary distribution of overdamped langevin equation in harmonic system. *Chinese Physics B*, 32(8):080501, jul 2023.
- [20] Kristina Maier, Martin Weiser, and Tim Conrad. Hybrid pde–ode models for efficient simulation of infection spread in epidemiology. *Proceedings of the Royal Society A: Mathematical, Physical and Engineering Sciences*, 481(2306):20240421, 2025.
- [21] Sadegh Marzban, Renji Han, Nóra Juhász, and Gergely Röst. A hybrid pde–abm model for viral dynamics with application to sars-cov-2 and influenza. *Royal Society Open Science*, 8(11):210787, 2021.

-
- [22] Sebastian Müller, Michael Balmer, William Charlton, Ricardo Ewert, Andreas Neumann, Christian Rakow, Tilmann Schlenker, and Kai Nagel. A realistic agent-based simulation model for covid-19 based on a traffic simulation and mobile phone data, 11 2020.
- [23] Sebastian A. Müller, Michael Balmer, William Charlton, Ricardo Ewert, Andreas Neumann, Christian Rakow, Tilmann Schlenker, and Kai Nagel. Predicting the effects of covid-19 related interventions in urban settings by combining activity-based modelling, agent-based simulation, and mobile phone data. *PLoS One*, 16(10), 2021.
- [24] John T. Nardini, Ruth E. Baker, Matthew J. Simpson, and Kevin B. Flores. Learning differential equation models from stochastic agent-based model simulations. *Journal of The Royal Society Interface*, 18(176):20200987, 2021.
- [25] Rylan Perumal and Terence L. van Zyl. Surrogate-assisted strategies: the parameterisation of an infectious disease agent-based model. *Neural Computing and Applications*, 37(2):627–638, 2025.
- [26] Jonathan Richard Shewchuk. Software triangle. <https://www.cs.cmu.edu/quake/triangle.html>.
- [27] Software ParaView. ParaView. <https://www.paraview.org>.
- [28] Kathleen M. Storey and Trachette L. Jackson. An agent-based model of combination oncolytic viral therapy and anti-pd-1 immunotherapy reveals the importance of spatial location when treating glioblastoma. *Cancers*, 13(21), 2021.
- [29] Çağlar Tozluoğlu, Swapnil Dhamal, Yuan Liao, Sonia Yeh, Frances Sprei, Devdatt Dubhashi, Madhav Marathe, and Chris Barrett. Synthetic sweden mobility (sysmo) model documentation, 07 2022.
- [30] Wikipedia contributors. COVID-19-Pandemie in Berlin. Accessed: 2024-11-07. https://de.wikipedia.org/w/index.php?title=COVID-19-Pandemie_in_Berlin&oldid=205195302.
- [31] Wikipedia contributors. COVID-19-Pandemie in Brandenburg. Accessed: 2024-11-07. https://de.wikipedia.org/wiki/COVID-19-Pandemie_in_Brandenburg.
- [32] Hanna Wulkow, T. O. F. Conrad, Natasa Djurdjevac Conrad, Sebastian Alexander Mueller, Kai Nagel, and Ch. Schütte. Prediction of covid-19 spreading and optimal coordination of counter-measures: From microscopic to macroscopic models to pareto fronts. *PLoS ONE*, 16(4), 2021.

Appendices

A Landscape Creation

A.0.1 25% Population

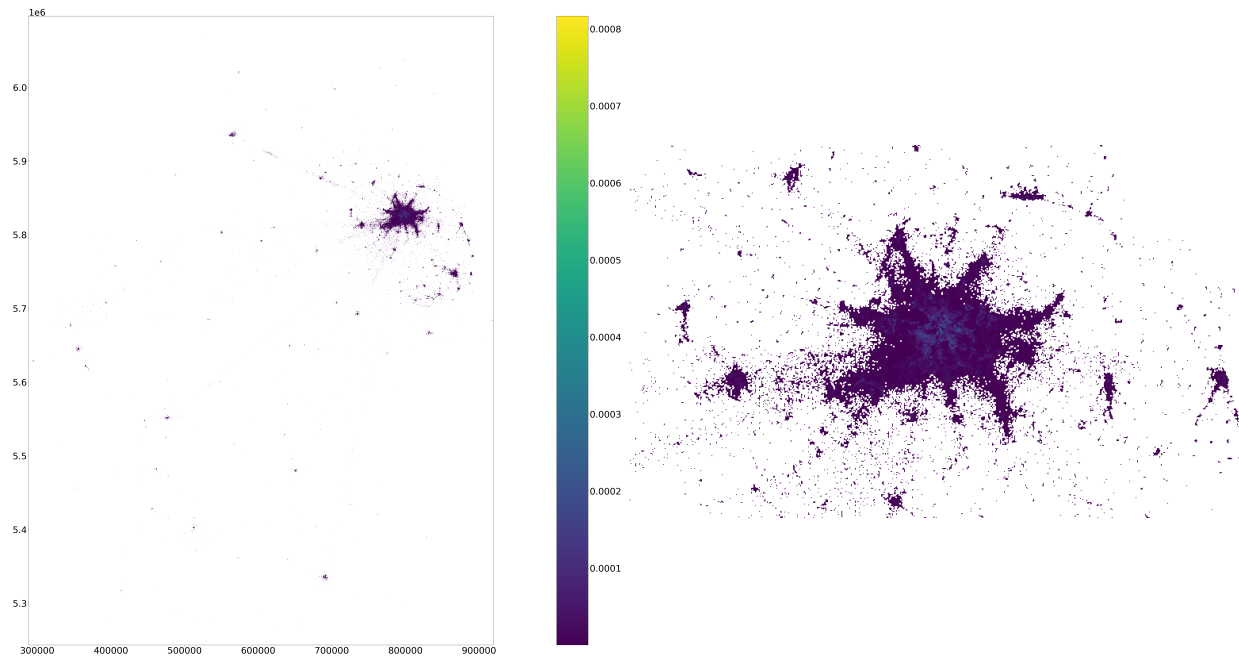


Fig. 15. Distribution of all agents (25% population) across Germany for a whole week as a histogram, including NaN values. White color corresponds to NaN values, indicating that no agent has ever been at these coordinates. Right: Close up Berlin-Brandenburg. The close-up images were manually centered and therefore do not align perfectly.

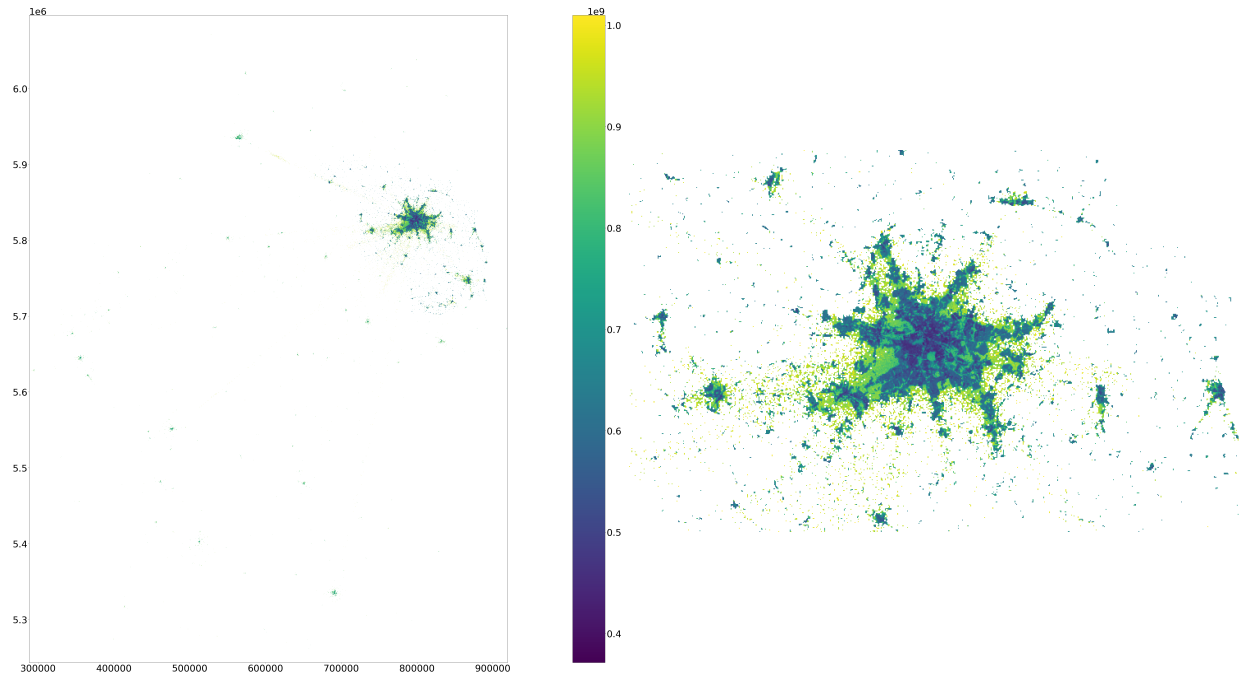


Fig. 16. Landscape of agent distribution (25% population) across Germany over an entire week, including NaN values. White color corresponds to NaN values, indicating that no agent has ever been at these coordinates. Right: Close up Berlin-Brandenburg. The close-up images were manually centered and therefore do not align perfectly.

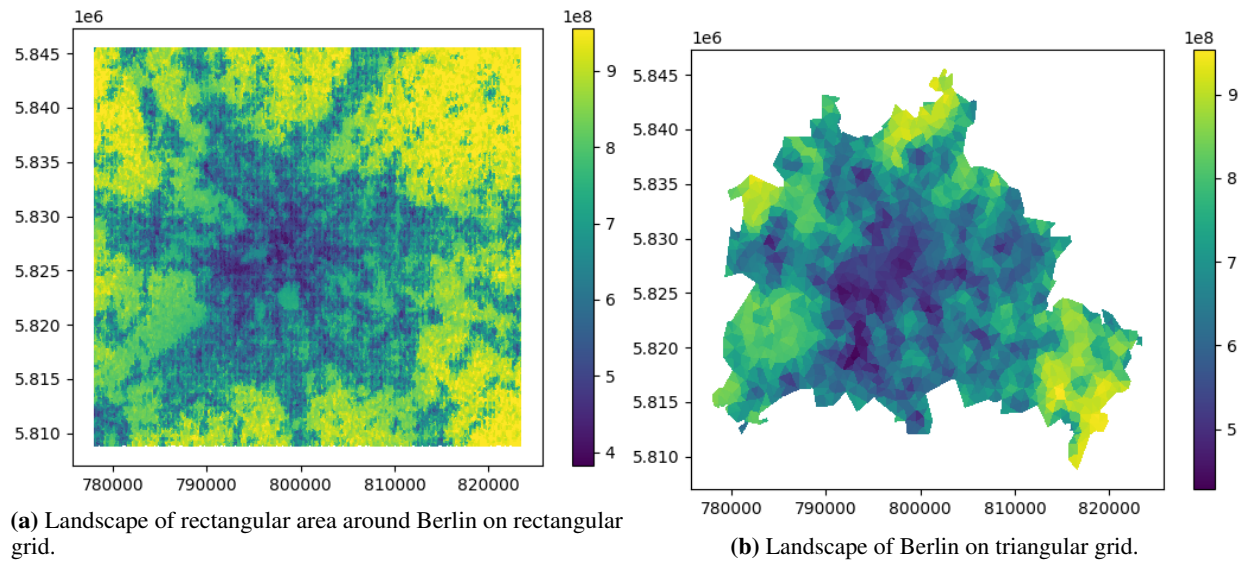


Fig. 17. Landscape of agent distribution (25% population) across Berlin over an entire week. Coordinates never visited by agents (NaN values) were set to the maximum value.

A.0.2 100% Population

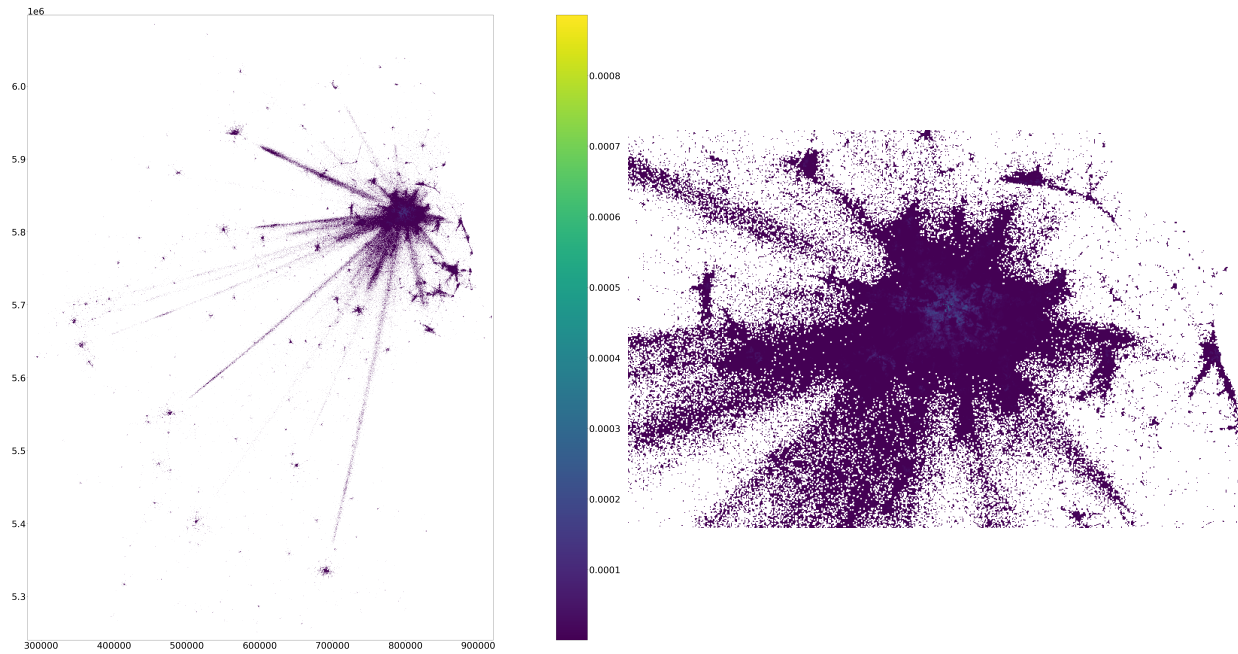


Fig. 18. Distribution of all agents (100% population) across Germany for a whole week as a histogram, including NaN values. White color corresponds to NaN values, indicating that no agent has ever been at these coordinates. Right: Close up Berlin-Brandenburg. The close-up images were manually centered and therefore do not align perfectly.

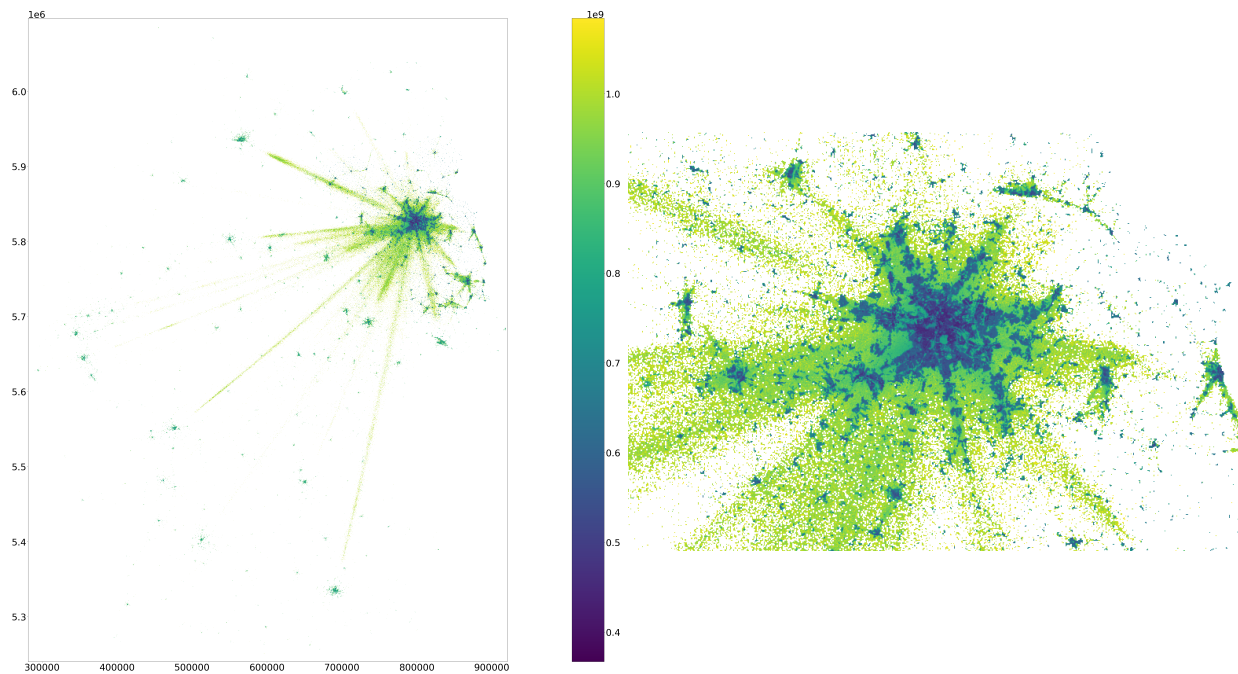


Fig. 19. Landscape of agent distribution (100% population) across Germany over an entire week, including NaN values. White color corresponds to NaN values, indicating that no agent has ever been at these coordinates. Right: Close up Berlin-Brandenburg. The close-up images were manually centered and therefore do not align perfectly.

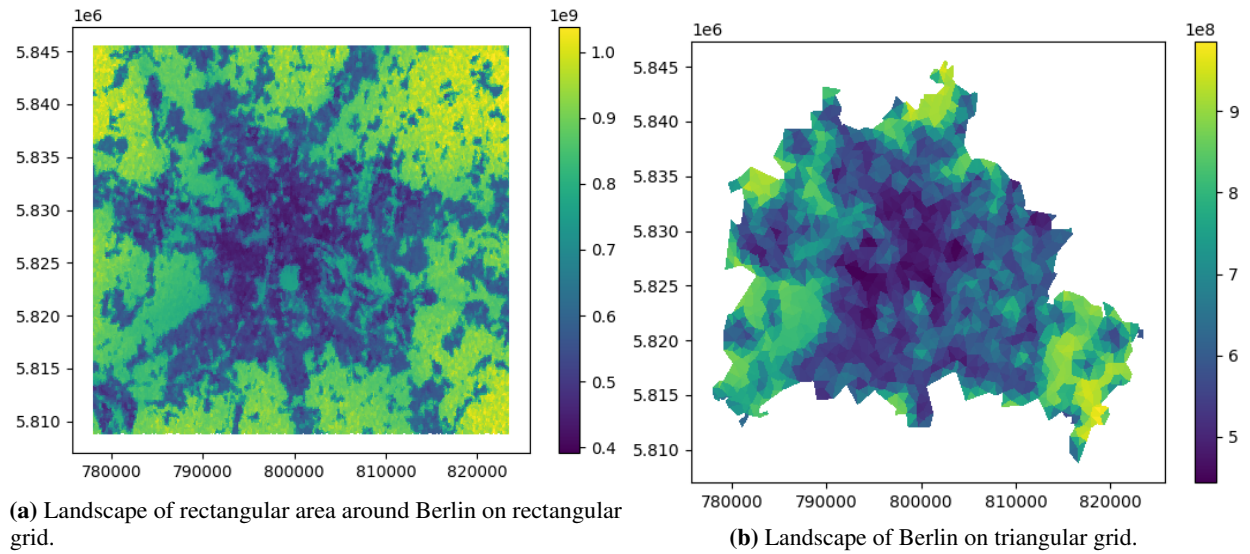


Fig. 20. Landscape of agent distribution (100% population) across Berlin over an entire week. Coordinates never visited by agents (NaN values) were set to the maximum value.